Award Accounts

The Chemical Society of Japan Award for Creative Work for 2002

Time-Resolved Thermodynamic Properties of Intermediate Species during Photochemical Reactions

Masahide Terazima

Department of Chemistry, Graduate School of Science, Kyoto University, Kyoto 606-8502

Received August 20, 2003; E-mail: mterazima@kuchem.kyoto-u.ac.jp

Thermodynamics and kinetics are very large and important fields in science. However, experimental efforts to link these two fields have been very limited so far. For instance, although the themodynamical properties of transient species are essential for the knowledge of the nature and energetics of the reaction, such data have been very scarce. Kinetic study of a reaction from a view point of thermodynamic properties in the time domain should be very useful to detect a spectrally silent kinetic property. We have developed experimental methods to measure the time development of the thermodynamical properties of transient species without any assumption and without any temperature or pressure variations. Some of the results, in particular applications to reactions of biological proteins (photodissociation of the ligand of carboxymyoglobin, photo-reaction of Photoactive Yellow Protein (PYP) and octopus rhodopsin), are reviewed.

Thermodynamics has been playing very important roles in science to reveal the nature of molecules or the state of substances. The thermodynamical properties; molecular volume, enthalpy, entropy, free energy, thermal expansion coefficient, sound velocity, and so on have been considered to be fundamental properties to describe the states. Because of this importance, a variety of techniques to measure these quantities have been developed and a number of valuable data have been accumulated. Besides assisting in understanding the nature of stable molecules, these properties has been used for elucidating the changes of states; i.e., chemical reactions. Indeed, thermodynamical studies have been reported for a number of equilibrium reactions under various conditions. For example, the volume change (ΔV) and enthalpy change (ΔH) of a reaction have been measured mainly by the hydrostatic pressure (p) and temperature (T) dependencies of an equilibrium constant (K) using the relationships;[1–5]

$$k_B(\partial \ln K/\partial(1/T))_p = \Delta H \qquad (1)$$
$$-k_B T(\partial \ln K/\partial p)_T = \Delta V$$

where k_B is the Boltzmann constant. These properties are important, because they reflect both the molecular structures and the intermolecular interactions.

On the other hand, a variety of time-resolved spectroscopic studies have revealed intermediate species (or states) during many chemical reactions on a very wide time scale. The nature of the intermediate species is a key factor to understand the reactions and they actually control the reactions in many cases. Spectroscopic methods for the investigation of reaction kinetics are now well developed. Although reaction kinetics and thermodynamics are wide and mature fields, experimental efforts to link these two fields have been very limited. Contrary to the well-developed time-resolved spectroscopies, a difficulty we encounter in studying chemical reactions based on thermodynamics is the fact that the thermodynamical properties are not easily accessible for transient species. For instance, the above traditional methods for the measurement of ΔH and ΔV, temperature or pressure dependence measurements, cannot be applied to irreversible reactions. The effect of pressure or temperature on the rate constant provides us only the activation volume ($\Delta V^{\ddagger}$) or the activation enthalpy ($\Delta H^{\ddagger}$), respectively. The reaction volume (ΔV) can be determined only by measuring the partial molar volumes of the product and reactant individually, and naturally this method cannot be applied to short-lived transient species. One challenge facing chemists studying chemical reactions is to obtain thermodynamic information about the intermediate states involved in rapid reactions (Fig. 1).

The transport properties are another important factor for understanding the role of the molecular conformation and intermolecular interaction. However, the measurement of the diffusion coefficient (D) in time-domain has been also very difficult or almost impossible for transient species by traditional techniques such as NMR, Taylor dispersion, or capillary methods.[6,7] The transport property of unstable intermediate biological molecules was not elucidated at all.

Recently our group has been working on the time-resolved studies of thermodynamical as well as transport properties during a variety of photophysical processes and photochemical reactions. The studies include ultrafast detection of temperature increase after the nonradiative transition,[8] time-resolved detec-

Published on the web January 13, 2004; DOI 10.1246/bcsj.77.23

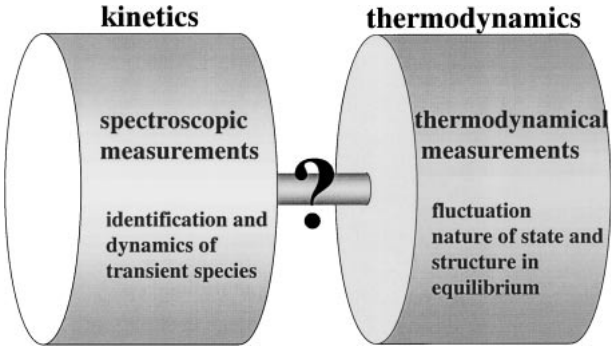

Fig. 1. Kinetics and thermodynamics are large and important fields (wheels) in science. The linkage between these wheels is now constructing.

tion of enthalpies and volume changes without any temperature or pressure variation,[9,10] and the time-resolved detection of diffusion processes of transient organic radicals and the excited triplet state molecules.[11] For example, we developed four new methods: temperature lens, temperature grating, an acoustic peak shift method, and molecular heater–molecular thermometer system, to reveal elementary processes of the energy conversion from the molecular energy to the thermal energy. The studies on time-resolved diffusion process of transient radicals provide us rich knowledge about the intermolecular interaction of unstable radicals in solution phase as well as the reaction kinetics.[11] Some topics have already been reviewed and discussed in other articles.[12,13] In this Account, we review the time-resolved thermodynamical measurements of some biological proteins performed in our group.

The thermodynamical properties are of importance for biological molecules.[14] If we can measure the thermodynamical properties for the transient species during chemical reactions, the accumulated data for stable molecules enable us to understand these reactions much more deeply. For example, the partial molar volume of a protein is a macroscopic observable, but this property is particularly sensitive to the hydration of solvent-exposed atomic groups as well as to the structure, dynamics and conformational properties of the solvent, and such results provide us useful information on the molecular nature of the protein.[15,16] However, as stated above, little information has been obtained for short-lived reaction intermediates. A unique way for the measurement of ΔH of unstable intermediate species, in particular for biological macromolecules, is the direct calorimetric technique by trapping an unstable species at a low temperature. Cooper and co-workers utilized this technique to reveal the enthalpy changes associated with kinetic steps of several photoreactive systems, such as bovine rhodopsin[17] and octopus rhodopsin.[18] The data from their group have been used frequently for analyzing or interpreting biological reactions.[19,20] However, we should always worry about the possibility that the enthalpy changes of the cryogenically trapped species could be different from those of the real intermediate species at ambient temperature during the reaction, because the conformational changes of the chromophore, peptide backbone and water molecules should be suppressed at a low temperature. These values could also be temperature-dependent. Preferably, the thermodynamical properties during a chemical reaction in the time domain should be measured under a physiological condition.

As a link between thermodynamics and kinetics (Fig. 1), we stress that measurement of volume or energy changes in the time domain opens up a new and interesting area for kinetic studies. Reaction kinetics has been mostly studied spectroscopically in the visible or UV range, monitoring the change of the chromophore's absorption. If the reaction changes the absorption that is monitored, one can detect all of the kinetics in the reaction. However, if the reaction does not influence the absorption at least in an experimentally accessible wavelength region, the kinetics are spectrally silent. Even in such cases, the kinetics can be monitored by detecting the time dependence of the energy and/or volume changes. This should be an interesting field, particularly for kinetic studies on macromolecules or biological materials.

One of the techniques that enables us to access these quantities for irreversible reactions is photoacoustic (PA) spectroscopy, which is sometimes referred as photoacoustic calorimetry, time-resolved photoacoustic calorimetry, or laser-induced optoacoustic spectroscopy.[21–26] This is a well-established powerful method to detect pressure waves after photoexcitation; such waves are created mainly by the thermal expansion of the medium and by molecular volume changes. Although the PA method is a powerful technique, there are still some inherent limitations: ΔH and ΔV should be determined under an assumption (vide infra). We have used the pulsed laser induced transient grating (TG) and transient lens methods for quantitative measurements of the molecular volume change (and partial molar volume) and the enthalpy change during a photochemical reaction in time domain without any assumption for the first time. These methods allow a kinetic description of both the energetics and the conformational changes that occur during chemical and biological transformations. Furthermore, the temperature dependence of ΔV provides the change in the thermal expansion coefficient ($\Delta\alpha$) by the reaction. Since this $\Delta\alpha$ is proportional to the cross correlation between the volume and entropy fluctuations,[27,28] this information is valuable for revealing the importance of structural fluctuations during chemical reactions.

The diffusion coefficient (D) can also be measured with a 10 μs time resolution by using the TG technique, so that D of a short-lived state during this time range can be studied.[11] Therefore, we are now able to access the thermodynamic properties and the transport property of unstable intermediate species of proteins during a biological reaction. In this Account, I describe the time-resolved thermodynamical properties as well as the diffusion coefficients of intermediate species during the photocyclic reaction of photoactive yellow protein (PYP), myoglobin, and rhodopsin.

1. Principles

The time-resolved measurement of the thermodynamical properties is based on the transient grating (TG) techique. In the TG method, a sample is photoexcited by an optical interference pattern between two beams crossed at a point within the coherence time.[29–33] By assuming that the amplitudes of the two light fields are equal, one may write the intensity as

$$I(x,t) = 2I_0 f(t)[1 + \cos(qx)] \quad (2)$$

where x is a spatial coordinate along the grating wave vector, $f(t)$ is the temporal profile of the beam, I_0 is the laser power, and q is the grating wavenumber. Illumination of a sample by this light induces a spatially modulated concentration profile of excited-state molecules. Following this photoexcitation, photophysical and photochemical processes take place. These processes create a sinusoidal modulation in the refractive index (n) and the absorbance (k) caused by various factors discussed later. The grating is monitored by use of the diffraction of a cw probe beam. For a thick grating, the probe is brought in at an appropriate angle to satisfy the phase-matching condition (the Bragg condition). Under a weak diffraction condition, the grating intensity (I_{TG}) is approximately proportional to the square of the variations in the refractive index (δn) and absorption (δk):[31]

$$I_{TG} \cong \alpha(\delta n)^2 + \beta(\delta k)^2 \quad (3)$$

where α and β are constants that represent the sensitivity of the system.

There are various causes of changes in the refractive index or absorbance induced by light irradiation.[32,33] Under normal experimental conditions for studying photochemical reactions, the refractive index change mainly consists of the following three components.

1. After the nonradiative transition of the excited states, the temperature is raised by the released energy, and the density of the matrix is altered by the heating effect, which creates the thermal grating (δn_{th}). The magnitude of the thermal grating of a calorimetric reference sample ($\delta n_{th}{}^{R}$) is given by

$$\delta n_{th}{}^{R} = (dn/dT)NWh\nu/(C_p\rho) \quad (4)$$

where dn/dT is the temperature dependence of the refractive index of the solution, $h\nu$ is the photon energy of the excitation light ($J\,mol^{-1}$), N is the number of the excited molecules per unit volume (mol/cm^3), W is the molecular weight ($g\,mol^{-1}$), ρ is the density (g/cm^3), and C_p is the heat capacity at a constant pressure ($J\,mol^{-1}\,K^{-1}$). If the amount of the released heat is changed by a factor ϕ due to a chemical reaction, the refractive index change of the sample (δn_{th}) should be changed by the same amount:

$$\delta n_{th} = (dn/dT)\phi NWh\nu/(C_p\rho) \quad (5)$$

The fraction of energy released as heat may be given by $\phi = 1 - (\Phi\Delta H/h\nu)$, where ΔH is the enthalpy change of the reaction and Φ is the quantum yield of the reaction.

We can determine $\Phi\Delta H$ by a comparison of the TG signal intensity of a sample with that of a calorimetric reference under the same experimental conditions. The ratio of the refractive index change for the sample (δn_{th}) to that for reference ($\delta n_{th}{}^{R}$) under the same experimental conditions is given by

$$\delta n_{th}/\delta n_{th}{}^{R} = \phi \quad (6)$$

When the rate of the chemical reaction is not fast enough compared with $D_{th}q^2$, the time evolution of the heat releasing process ($Q(t)$) should be taken into account and the time profile of the thermal grating signal intensity is given by

$$\delta n_{th}(t) = (dn/dT)(W/(C_p\rho))dQ(t)/dt^{*} \exp(-D_{th}q^2t) \quad (7)$$

where * denotes the convolution integral. Hence we can measure the time dependence of the enthalpy change during reactions.

2. The refractive index change induced by a molecular polarizability difference between the reactant and product molecules due to the change of absorption spectrum is called the population grating (δn_{pop}). The population grating is related to the change in the absorption spectrum by the Kramers–Kronig relation.[34] The refractive index due to the i-species (δn_i) is related to the molecular polarizability (α_i) by the Lorenz–Lorentz relation as follows:[9,10]

$$\delta n_i = ({n_0}^2 + 2)^2 N(\alpha_i - (V_i/V_{solv})\alpha_{solv})/18n_0\varepsilon_0 \quad (8)$$

where V_i and V_{solv} are the partial molar volumes of the i-species and the solvent molecule, respectively, α_i and α_{solv} are the molecular polarizabilities of the i-species and solvent, n_0 is the unperturbed refractive index of solution and ε_0 is the vacuum permittivity. We can decompose this contribution into the polarizability term of the i-th molecule (δn_{pop}) and the molecular volume term. The former may be written as

$$\delta n_{pop} = ({n_0}^2 + 2)^2\alpha_i N/18n_0\varepsilon_0 \quad (9)$$

3. The density change caused by the reaction volume change gives rise to the volume grating (δn_{vol}). The contribution from the i-species with a partial molar volume of V_i is given by

$$\delta n_{vol\text{-}i} = ({n_0}^2 + 2)^2\alpha_{solv}NV_i/18n_0\varepsilon_0V_{solv} \quad (10)$$

Hence, by isolating the volume grating in the signal, we can measure not only the volume change but also the partial molar volume.

We often call the sum of δn_{pop} and δn_{vol} the species grating (δn_{spe}), because the time profiles of δn_{pop} and δn_{vol} are identical for most cases. Quantitative measurement of these contributions allows us to determine the amount of the thermal energy released by the sample, the absorption change at the probe wavelength, and the volume change in the time-domain.

When the signal consists of thermal and species contributions simultaneously, these contributions should be separated for quantitative measurements. We can use the temperature dependence or the solvent dependence methods for changing the solution properties. While δn_{th} is proportional to dn/dT of the solution (Eqs. 4 and 5), the volume contribution does not depend on this quantity. Since dn/dT of water strongly depends on the temperature (it vanishes around 0 °C), the temperature dependence method can be used for aqueous solution. If we can plot the signal intensity versus dn/dT without changing the other physical and photochemical properties of the solute, ΔH can be determined from the slope of the plot and the species grating contribution from the intercept. One can also vary dn/dT by varying the solvent among a series of alkanes or by mixing two solvents, which should not change the other molecular properties of the solute. These methods have been frequently used in studies using the PA method.[23,26] The solvent dependence method was demonstrated for the TG method by Morais et al. to separate the thermal contribution from the others.[35]

Aside from these rather 'traditional' techniques, there is a unique way to separate the thermal contribution from the others by means of the TG method. The separation can be accomplished based on the characteristic decay rate of the thermal contri-

bution, explained as follows.[9,10] The time evolutions of the thermal and species grating intensities depend on the heat-releasing kinetics and reaction kinetics, as well as on the diffusion process within the fringe pattern. The TG signal from this grating is expressed by[11]

$$I_{TG}(t) = \alpha\{\delta n_{th}\exp(-D_{th}q^2t) + \Sigma\delta n_p\exp(-D_pq^2t) - \Sigma\delta n_r\exp(-D_rq^2t)\}^2 + \beta\{\Sigma\delta k_p\exp(-D_pq^2t) - \Sigma\delta k_r\exp(-D_rq^2t)\}^2 \quad (11)$$

where the subscripts p and r stand for the product and the reactant, respectively, and $\delta n_{p(r)}$ and $\delta k_{p(r)}$ are the peak-to-null refractive index and absorbance difference at $t = 0$, respectively. The negative signs for δn_r and δk_r represent the 180° phase shift of the fringe pattern versus that of product due to the consumption of the reactant. Since D_{th} is generally much larger (ca. 2 orders of magnitude in a typical case) than $D_{i(j)}$ in solution, the thermal component can be separated from the species grating signal by the time-resolved manner, which allows us to determine ΔH of the reaction by a comparison with the intensity of the thermal signal of a reference sample.

The molecular volume change can be determined from the acoustic wave after the photoexcitation. Detection of the acoustic wave can be achieved in two ways: either by use of the acoustic component of the TG signal or by use of the PA method. When the heat is released and the molecular volume is changed fast enough compared with the acoustic transit time and the excitation laser pulse, an acoustic wave is clearly observed in the first part of the TG signal. The peak-to-null intensity of the acoustic oscillation is related to the density change that is caused by the release of the heat and reaction volume change. If ΔH of the reaction is already determined by the method described above, ΔV can be determined from the intensity of the acoustic oscillation. Alternatively, the acoustic wave can be detected by the PA method (TG–PA hybrid method).

2. Results and Discussion

2-1. Diphenylcyclopropenone (DPCP). For showing how the TG (or TG–PA) method works, we first describe an example of the TG application to a simple photo-irreversible chemical reaction: the photodissociation reaction of diphenylcyclopropenone (DPCP).[9,10] After photoexcitation of DPCP, it dissociates to yield CO and acetylene. This reaction is complete within a few ps after the photoexcitation, and the quantum yield is unity in alkanes.[36,37] Because of the simple and clean reaction as well as the strained molecular structure, the reaction volume and the enthalpy change of this reaction have been investigated by a number of groups.

Figure 2 shows the TG signals after the photoexcitation of DPCP on different time scales.[9,10] The signal rises within 50 ns after the excitation and decays monotonically. The time profile of the signal was expressed well with a tri-exponential function:

$$I_{TG}(t) = \{a_f\exp(-k_ft) + a_i\exp(-k_it) + a_s\exp(-k_st)\}^2 \quad (12)$$

Since the decay rate constant of the fastest component, k_f, was $D_{th}q^2$, it should be attributed to the thermal grating signal. The other, intermediate and slow, components should originate from the chemical species. Considering the chemical species involved in the reaction, one may expect that the time profile of the species grating can be expressed by

$$I_{TG}(t) = \alpha\{-\delta n_{DPCP}\exp(-D_{DPCP}q^2t) + \delta n_{CO}\exp(-D_{CO}q^2t) + \delta n_{ace}\exp(-D_{ace}q^2t)\}^2 \quad (13)$$

where the subscripts DPCP, CO, and ace stand for DPCP, CO, and acetylene, respectively. From the magnitude of D and the size of the molecules, it is rather easy to assign the intermediate component (k_i) to the contribution of CO, and the slow one (k_s) to the sum of DPCP and acetylene.

First, by subtracting the species grating contribution from the observed TG signal, the pure thermal grating intensity was obtained, and ΔH was determined from the intensity (Fig. 2(a)). Next, the contributions of δn_{pop} and δn_V were separated into two from the acoustic signal intensity and ΔH (Fig. 2). From the magnitude, the total volume change during the reaction was determined. Hence, ΔH and ΔV of the irreversible reaction in one solvent at one temperature under one pressure were measured without any assumption for the first time. Furthermore, the species grating signal could be clearly decomposed into two contributions, CO and acetylene + DPCP, because they have different diffusion coefficients (Fig. 2(b)). These signals consist of δn_{pop} and δn_v. Subtracting δn_{pop} calculated accurately enough for CO from the data of the refractive index, we obtained the partial molar volume of CO ($\bar{\mathbf{V}}_{CO}$) at the same time. For example, ΔH, ΔV, and $\bar{\mathbf{V}}_{CO}$ in hexane were, respectively, 10.1 kJ/mol, 38.5 cm^3/mol, and 45.3 cm^3/mol. These quantities in nonane were 7.5 kJ/mol, 32.4 cm^3/mol, and 38.9 cm^3/mol, respectively. By using the same method, ΔV and ΔH in a micellar aqueous solution were determined at 20 °C. Comparing with the calorimetric reference sample and taking into account the result that the quantum yield of the photodissociation of DPCP in water is 1.0, we found that ΔH and ΔV in the aqueous solution were $\Delta H = 9.2\ kJ\ mol^{-1}$ and $\Delta V = 23$ cm^3/mol. Apparently, H, ΔV, and $\bar{\mathbf{V}}_{CO}$ depend on the solvent.

The volume change and enthalpy change of this reaction had been reported by the PA method before our TG study. In 1984, Grabowski et al. measured the PA signal after the photoexcitation of DPCP and compared it with that of a calorimetric standard sample.[38] They reported ΔH (heat of formation) of photodissociation of DPCP in benzene to be −41 kJ/mol, without considering the volume change contribution in the signal. Apparently, this ΔH is underestimated by neglecting the volume change contribution. Herman and Goodman measured ΔH and ΔV for the dissociation reaction of DPCP by means of the PA method in binary mixtures (acetonitrile (AcN)/water) and in a micellar solution with the temperature dependence strategy.[39] They obtained $\Delta H = 17.5$ kJ/mol and $\Delta V = 65.0$ cm^3/mol for the AcN/water mixture solution and $\Delta H = 10.4$ kJ/mol and $\Delta V = 60.1$ cm^3/mol for the micellar aqueous solution. The separation method of the volume and energy contributions using a series of alkanes was applied to the photodissociation reaction of DPCP by Hung and Grabowski for the first time.[40] They obtained $\Delta H = -28$ kJ/mol and $\Delta V = 23$ cm^3/mol. Schmidt and Schütz re-examined this reaction by the PA method in a series of alkanes at a constant temperature and with

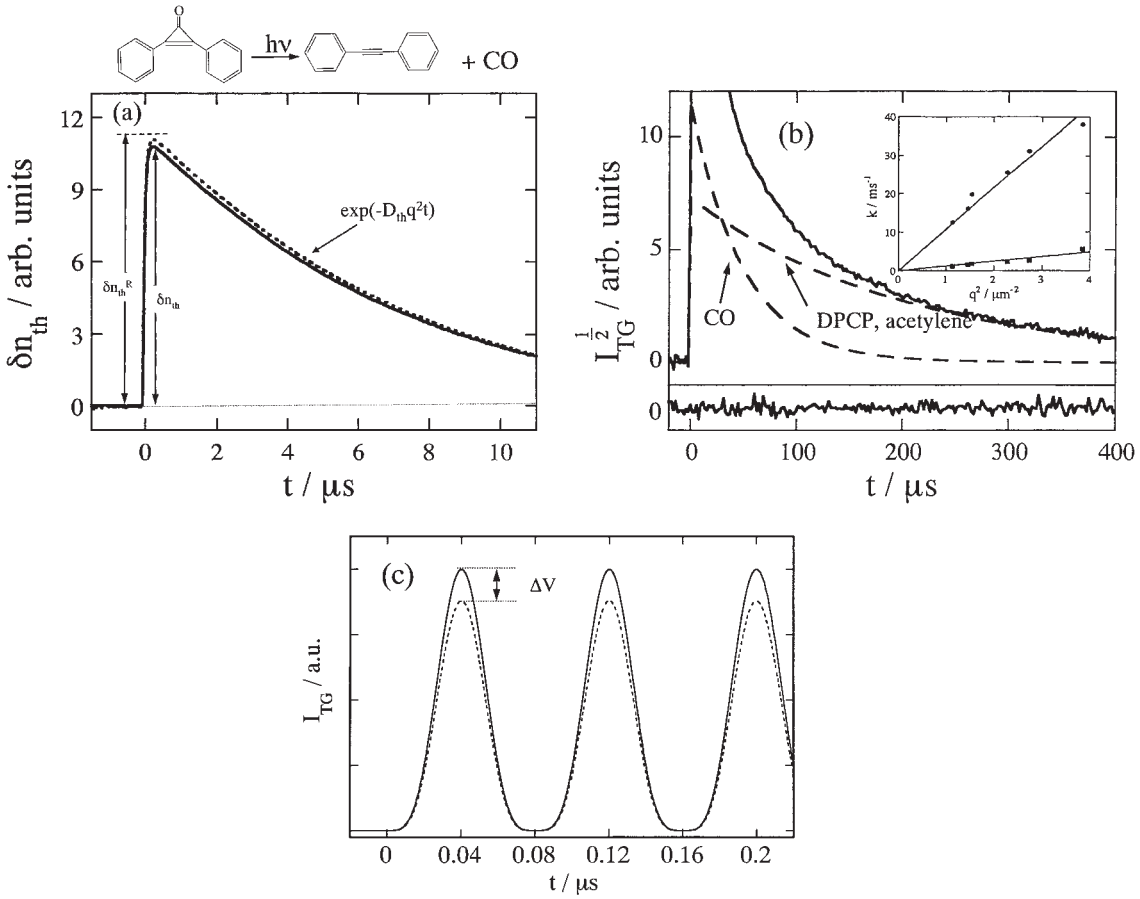

Fig. 2. (a) Square root of the TG signal due to the purely thermal grating of DPCP (solid line) and that from the reference sample (nitrobenzene) (dotted line) in heptane. (b) The TG signal after the photodissociation of DPCP in a longer time. The thermal component decays faster than the species components and it is not observed clearly on this time scale. Contributions of CO and (diphenylacethylene + DPCP) are decomposed by a bi-exponential fitting and are shown by the broken lines. The residual of the fitting is shown in the insetted (bottom). The upper right inset is the plot of the decay rate constants (k) vs the square of the grating number (q^2) showing that the decay rate constant is determined by the molecular diffusion process (circles, fast component; squares, slow component). (c) TG acoustic signal of DPCP (solid line) and that of the reference sample (dotted line). The intensity represents the thermal expansion of the medium and the molecular volume change. The reaction scheme of DPCP is shown in the upper part of (a).

the temperature variation method in aqueous solution with the careful elimination of possible error sources[41] and obtained $\Delta V = 22.3$ cm^3/mol and $\Delta H = -18$ kJ/mol in alkanes and $\Delta V = 22.1$ cm^3/mol and $\Delta H = -25$ kJ/mol in micelles. All of these PA studies were based on the assumption that ΔH and ΔV do not depend on temperature or solvent. However, as stated above, since ΔH, ΔV and the partial molar volume actually depend on the solvent and temperature, the discrepancy between the results from the TG and PA methods may come from the incorrect assumptions in the PA measurement.

In general, the assumption of temperature and solvent independence of ΔH and ΔV is difficult to be tested by the PA method, and the conditions are not satisfied sometimes. In particular, some temperature dependence of ΔV has been found for some biological proteins as shown below. Hence the TG method for measurement of ΔH and ΔV without this assumption is certainly very unique and useful for the time-resolved study of thermodynamical properties.

2-2. Photoactive Yellow Protein (PYP). PYP is a relatively new protein isolated from the purple sulfur bacterium *Ectothiorhodospira halophila*.[42] It is considered to possess a function of a blue light photoreceptor for a negative phototactic response.[43] It is a relatively small (14 KD) water-soluble protein; the protein structure was determined by the X-ray crystallography in 1.4 Å resolution.[44] The chromophore of PYP is 4-hydroxycinnamic acid covalently bound to the side chain of Cys69 via a thioester linkage.[45,46] Interests in the photophysical and photochemical processes of PYP are rapidly increasing recently, because it is a simple model for studies of signal transduction systems. After the photoexcitation, PYP shows a complete photocycle triggered by the photoisomerization of this chromophore.[47,48] Upon flash excitation of the chromophore, the ground state (pG, $\lambda_{max} = 446$ nm) is converted into a red-shifted intermediate (pR, $\lambda_{max} = 465$ nm) in less than 2 ns.[48] Subsequently pR decays in the sub-millisecond time scale into blue shifted intermediate (pB, $\lambda_{max} = 355$ nm), which returns to pG in a sub-s time scale.[47–49] Soon after the protein structure was revealed by the X-ray crystallography,[44,45] the time-resolved X-ray scattering experiments were performed.[50,51] They showed that the pR state possesses the cis conformation of chromophore and that the process of trans to cis isomerization was accompanied by the specific formation

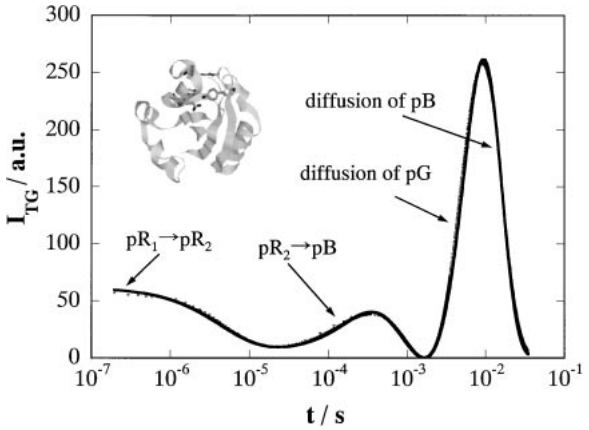

Fig. 3. Temporal profile of the TG signal of PYP solution (10 mM Tris–HCl buffer) excited at 465 nm (dotted line). Solid line is the best fitted curve using the method described in text. The assignments of the kinetic components are labeled in the figure.

of new hydrogen bonds. In the pB state, the phenolic oxygen of chromophore moves from the hydrophobic core of protein to become solvent-exposed and protonated.[50] According to these studies, the structural changes after light activation were localized near the chromophore. However, these structural changes were questioned recently by the studies using NMR spectroscopy[52] and IR spectroscopy[53] in solution. These studies show that the dynamics of PYP in solution is more global in the whole protein structure. Here I will show the thermodynamical properties and D of intermediate species of PYP reaction, which also indicated a global structural change.

(a) TG Signal of PYP: Figure 3 depicts the TG signal of the PYP solution after excitation at 465 nm.[54,55] The signal rises quickly after the excitation, then slowly with about 1 μs-time constant, and decays with a lifetime of several microseconds, which depends on the grating wavenumber. After the decay, the signal shows a growth–decay feature twice during a few milliseconds time scale. From the measurement at different grating wavenumbers (q), we found that the decay of the thermal grating and the kinetics of the second growth–decay signal depend on q, while the other two rate constants (k_1 and k_2) do not depend on q. Since there is no optical absorption from the original species (pG) nor from any intermediates of PYP at the probe wavelength (633 nm), the observed TG signal must come from the refractive index change after the photo-excitation. We found that the TG signal in the entire region can be well reproduced by the square of the summation of six exponential functions:[54,55]

$$\begin{aligned} I_{TG} = \alpha\{&\delta n_s \exp(-k_s t) + \delta n_{th} \exp(-q^2 D_{th} t) \\ &+ \delta n_1 \exp(-k_1 t) + \delta n_2 \exp(-k_2 t) \\ &+ \delta n_{pG} \exp(-q^2 D_{pG} t) + \delta n_{pB} \exp(-q^2 D_{pB} t)\}^2 \end{aligned} \quad (14)$$

where k_s is the rate constant of the slow rising component, as described in the next section in detail, and D_{pG} and D_{pB} are the diffusion coefficients of pG and pB, respectively. The kinetics which does not depend on q (k_1 and k_2) should represent the reaction dynamics of PYP. Considering the time scale, this dynamics should be the pR → pB process. The kinetics of pR → pB can be monitored by the transient absorption technique as reported previously.[46,47] The temporal profile associated with the pR → pB transformation can be fitted with lifetimes of 170 μs and 1.0 ms.

(b) Spectrally Silent Dynamics: The slow rise with the rate constant of k_s was unexpected before this TG measurement, because the photoisomerization of the chromophore occurs very quickly (<2 ps) and the transient absorption signal showed no time dependence of pR after the 3 ns-dynamics until the 200 μs-kinetics for pR → pB.[48] We found that the main part of the slow-rising component is not due to the thermal contribution, but it should be due to either population grating or volume grating contribution or both. In the time profile of the TA signal, this dynamics is not present; a number of reports on the PYP dynamics studied by the flash photolysis method have never observed this dynamics at any visible wavelengths.[48] Hence, this is an optically silent dynamics. The presence of this dynamics in the TG signal indicates that there is an intermediate species between the creation of the usually described pR and pB states. The absorption spectrum of this species is the same as that of pR. We referred to this new species as pR_2, which is created from the initial species (pR_1) from pG. Hence the reaction scheme of PYP should be described as shown in Fig. 4. (In this figure, several pB species that cannot be distinguished spectroscopically are also shown.[49])

The dynamics that cannot be detected by the absorption method indicates that the structural change that appears in the grating signal is a conformational change distant from the chromophore site. Although the protein structure that affects the absorption spectrum of the chromophore is initially changed within 3 ns upon creation of pR_1, the other protein parts move with the rate constant of k_s. This observation may be the most direct evidence for a global change of the protein in pR. If this rising component comes from the volume change entirely, the volume change (ΔV) in this dynamics can be calculated from the intensity of this component, $\Delta V = +5$ cm^3/mol. From further measurements for some site directed mutants of PYP, we found that this spectrally silent dynamics is sensitive to any changes of amino acids located far from the chromophore.[56] This result of mutant dependence also supports the conclusion that this

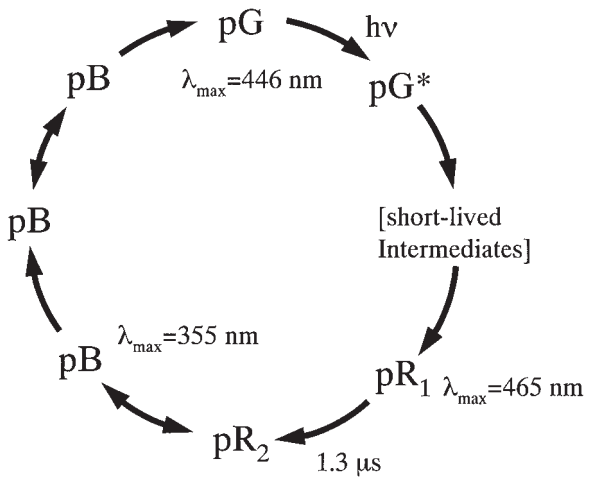

Fig. 4. Photocycle reaction of PYP at physiological temperature.

dynamics reflects the global movement of the amino acid residues.

(c) Enthalpy Changes: The second term of Eq. 14 represents the thermal grating signal. The intensity of this component should be proportional to the thermal energy released by the first step pG* → pR. The amount of the thermal energy is determined by the single exponential fitting from 1.5 μs after the photoexcitation. Comparing the thermal grating signal intensity with that of a calorimetric reference sample, we determined the stored energy in pR_2, i.e., the enthalpy change for pG → pR_2 (ΔH_1): $\Phi\Delta H_1 = 57 \pm 7$ kJ/mol. Using the quantum yield of the reaction $\Phi = 0.35$,[57] ΔH_1 is determined to be 160 ± 20 kJ/mol. (Two different quantum yields of the reaction were reported independently ($\Phi = 0.64$ by Meyer et al.;[47,48] $\Phi = 0.35$ by Van Brederode et al.[57] If we use $\Phi = 0.64$, ΔH_1 should be 90 ± 10 kJ/mol. ΔH and ΔV can be easily calculated from the values using $\Phi = 0.64$.) An advantage of this TG measurement is that we can quantitatively separate the energetic contribution (δn_{th}) in the signal without any assumption.

Since the decay of the thermal grating signal is generally much faster than the kinetics of pR → pB, the TG signal due to the thermal energy released by this process is too small to be determined. For studying the enthalpy of the pB state (ΔH_2), we used the TrL method. This method detects the refractive index change caused by the photoirradiation similarly to the TG method, but the excitation beam with a Gaussian spatial profle is used instead of the interference pattern for the TG method. The decay of TrL signal is in the order of tens milliseconds and the thermal energy releasing by the pR → pB process can be detected as a clear rise of the signal. Here, we used the traditional technique to separate the thermal intensity from the other contributions; the temperature dependence method. By comparing the thermal lens signal intensity with that of the calorimetric reference sample, we determine the enthalpy difference between pG and pB (ΔH_2). Again using $\Phi = 0.35$, we obtain $\Delta H_2 = 60 \pm 30$ kJ/mol (Fig. 5).

Our result for ΔH ($\Delta H_1 = 160$ kJ/mol, $\Delta H_2 = 60$ kJ/mol) clearly indicates that the energy of the pR state is astonishingly high and, that large energetic stabilization takes place during the pR → pB process. The time-resolved X-ray study[51] showed

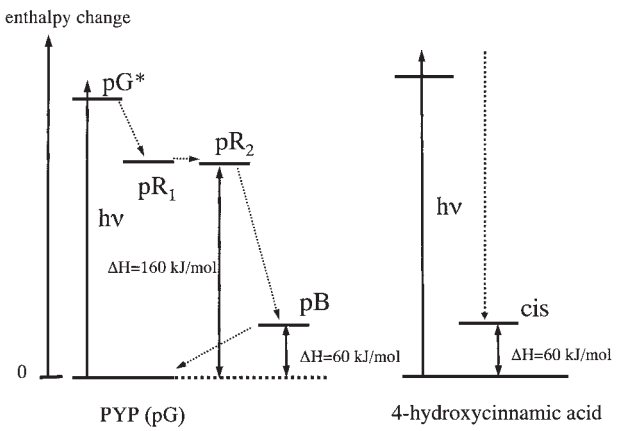

Fig. 5. Energy diagram of the photoreaction of PYP and the chromophore (4-hydroxycinnamic acid) obtained in time-domain at room temperature.

that the trans to cis isomerization is completed in less than 1 ns. From the energetic view, these facts suggest that the protein part has not yet relaxed in the pR_2 state to adopt the new conformation of the chromophore; that is, the protein structure is strained in pR. This strain may cause the large enthalpy of the pR species. It is reasonable to speculate that the following step (pR → pB) is driven by this energy stored in pR. In pB, the whole protein structure is relaxed to adopt to the cis form of the chromophore and this relaxation causes the lower enthalpy of pB. This feature is similar to the case of a typical visual signal transducer, the rhodopsin as described in a later section.[18,58] In this protein, the enthalpy is very high until batho intermediate (130 kJ/mol) and suddenly decreases to 50 kJ/mol in the next step.[18] From the energetic point of view, the pR state of PYP is similar to batho of rhodopsin.

It is interesting to note that the enthalpy difference between the trans- and cis-isomers of 4-hydroxycinnamic acid in water is about 50 kJ/mol. From this fact, the enthalpy of pB seems to come only from the unstable energy of the cis chromophore; i.e., the almost completely relaxed protein structure in pB. (However, we should note that the coumaric acid in pG is deprotonated and this chemical change should also be taken into account.)

(d) Volume Change: With ΔH_1 determined from the TG measurement and the PA intensities of the sample and the reference, we calculated $\Phi\Delta V$ associated with the pG → pR transformation. Using $\Phi = 0.35$, the volume contraction of $\Delta V = -7 \pm 2$ cm^3/mol was obtained at 20 °C.

The partial molar volume of a solute can be described as a sum of the following basic contributions:[16]

(1) constitutive volume, which is the sum of the van der Waals volumes of all the protein constitutive atoms;

(2) void volume: the volume of the structural voids within the solvent-inaccessible core of the protein that result from imperfect atomic packing (V_V);

(3) thermal motion contribution; a space required for heat motion at non-zero temperature;

(4) interaction volume. The effects of solute–solvent interactions caused by electrostriction around charged groups or by the hydrogen bonding of polar groups with water.

(5) Translational thermal motions of molecules ($\kappa_T k_B T$: κ_T, isothermal compressibility). Usually this is negligible in large molecules like protein.

The van der Waals volume is conserved during the reaction; hence, it does not contribute to the volume change here. It is interesting to note that the molecular volume change of the size of PYP usually is (slightly) negative during the native-to-unfolding process.[16] This contraction of the protein volume by the unfolding process has been explained by multiple contributions from the above factors as follows. The solvation of polar groups and charged groups cause a decrease in volume. In addition, the transfer of nonpolar groups from hydrophobic to aqueous environments such as occurs upon protein denaturation also causes a decrease in volume since the volume changes due to hydration are negative. The change in the void volume due to imperfect protein packing is also expected to be negative upon denaturation. On the other hand, 'thermal volume', which results from thermally induced molecular vibrations of both the solute and solvent molecules, thereby leads to an expansion of the solvent. These contributions cancel each other and, as a result, the

volume change upon unfolding for 'small' proteins is predicted to be small negative. The observed small volume contraction by the pR formation is consistent with this prediction, so we may speculate that the pR formation process can be considered as the denaturation process of the protein part. Based on this interpretation, since the average hydration contribution to the protein partial volume is proportional to the solvent-accessible surface areas of the protein: $\Delta V_h \propto S_A$, the negative volume change may suggest that the solvent-accessible surface areas increases by the pG $\rightarrow$ pR process. The partial molar volume change of pR, the pR state, may be interpreted as the unfolded protein structure.

(e) Thermal Expansion Coefficient of Transient Species: One of interesting observations in this PYP study was the temperature dependence of the volume change. From the species grating signal intensity and also from the PA intensity, ΔV was determined at various temperatures (Fig. 6). The partial molar volume changes in irreversible reactions in water have been measured mainly by the laser-induced PA method with an assumption that ΔV does not depend on temperature. Since there was no alternative way, this assumption has never been tested rigorously. Using the time-resolved TG and PA hybrid method, we could detect a rather large temperature dependent ΔV for the first time.[54]

The slope of the plot, ΔV vs T (Fig. 6), corresponds to $\Delta\alpha_{th}$ ($\Delta\alpha_{th} = (\partial\Delta V/\partial T)_p$), which is the change in the coefficient of thermal expansion for the initial (pG) and the intermediate (pR) forms (pR_1 and pR_2). This indicates that the thermal expansivity of pR is larger than that of pG. This is an interesting observation, not only because this is the first example to show the different α_{th} between the reactant and the reaction intermediate, but also because previous studies on the thermodynamical properties of proteins have already clearly showed that the partial molar volume of the unfolded state increases more significantly with temperature than that of the folded state.[59] Hence this observation, temperature-dependent ΔV, also indicates the resemblance of the pR state to the unfolded state of protein. The larger α_{th} for unfolded protein is intuitively understandable if one considers that the unfolded protein has a loose protein structure, which is expected to be sensitive to the temperature. In fact, α_{th} is proportional to the cross-correlation of the volume (V) and entropy (S) fluctuations,[27,28]

$$\langle SV - \langle S\rangle\langle V\rangle\rangle = kTV\alpha_{th} \tag{15}$$

where $\langle\ \rangle$ indicates the ensemble average and k is the Boltzmann factor. The larger α_{th} is an indication of larger structural and/or entropy fluctuations. Therefore, even in this initial intermediate species pR, which is created after 3 ns of the photoisomerization of the chromophore, the protein structure is loosened. Apparently, the structural change is not restricted to around the chromophore. The difference of α_{th} between the folded and unfolded metomyoglobin (metMb) was reported to be $\Delta\alpha_{th} = +2.4$ cm^3/mol·K,[60] while $\Delta\alpha_{th}$ for pG and pR of PYP was $+0.6$ cm^3/mol·K. If we tentatively assume that $\Delta\alpha_{th}$ for metMb is a typical value for $\Delta\alpha_{th}$ of the native and unfolded conformation, the pR conformation is about 25% unfolded from pG. We think that this value is too large as the indicator of the unfolded nature in pR. The time-resolved FT-IR experiment does not indicate such large backbone amide group movement in pR.[53] These results may suggests that the conformation of pR is not changed significantly from pG, but that the rigidity of the structure is weakened. Apparently, this weakening is caused by the strain induced by the photoisomerization of the chromophore as suggested from the large enthalpy of this species. This larger conformational flexibility in pR causes the next larger protein structural change in pR $\rightarrow$ pB.

From another point of view, this temperature-dependent ΔV_1 may be interpreted in terms of many possible local minima of the potential curve along the reaction coordinate. Many biological systems such as PYP are not rigid reaction systems but there are many local free energy minima (substates) along the reaction coordinate. This thermal fluctuation of the protein structure is essential for the biological function. The observed temperature-dependent volume change may reflect the structural fluctuation of the PYP protein structure.

(f) Diffusion Coefficient of Transient Species: The fifth and sixth terms in Eq. 14 should be attributed to the molecular diffusion process. As the identification of the diffusing species, there are two possibilities for the diffusion kinetics: $D_{pG} > D_{pB}$ or vise versa. We can identify the diffusing species from the signs of the pre-exponential factors and we found $D_{pG} > D_{pB}$. The time constants of two exponential functions ($D_{pG}q^2$, $D_{pB}q^2$) are plotted against q^2 (Fig. 7). From the slope of the least square fit of these plots, we obtained D of pG and pB as 1.21×10^{-10} m^2/s and 1.00×10^{-10} m^2/s, respectively. One of unique advantages of the TG detection is that the diffusion coefficients (D) of transient species can be measured.

We may notice that the observed 1.2 times difference between D_{pG} and D_{pB} is very large. From the Stokes–Einstein theory,

$$D = k_B T/a\eta r \tag{16}$$

where a is a constant depending on the boundary condition between the solute and solvent, k_B is Boltzmann constant, T is absolute temperature, η is viscosity of the solvent and r is radius of the solute, the volume of pB must be 1.2^3–1.7 times as large as the volume of pG, if the difference in D comes only from the volume change from pG to pB. If such a large volume expan-

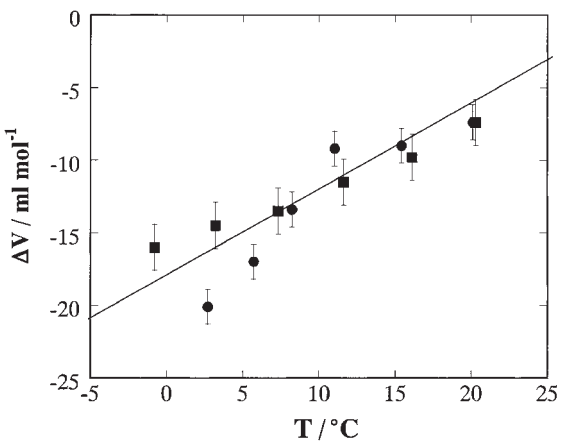

Fig. 6. Plots of the volume change (ΔV) of PYP determined from the intensity of the volume grating (squares) and PA signal (circles) at various temperatures. The line is a guide for eyes.

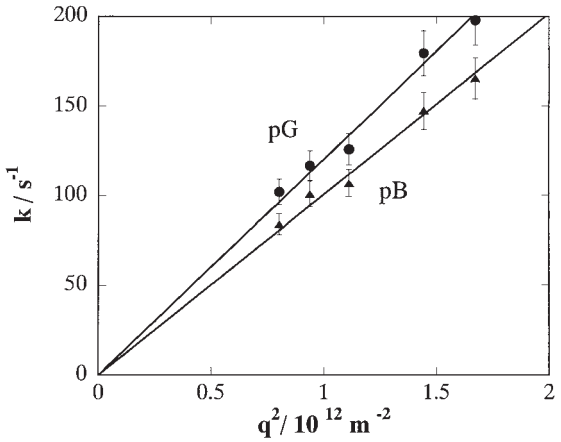

Fig. 7. The q^2 plots of the decay rate constant (k) of the two diffusion components in TG signal and the least-square fits (circles for pG; triangles for pB). The solid lines are least square fitting by the equation of $k = Dq^2$.

sion occurs, an extremely large δn_v component should be observed. Judging from the profile of TG signal, this is not the case. Therefore, we presume that this difference of the diffusion coefficient comes from the large change of interaction between the protein and water molecules in pG and pB.

For the interpretation of the fact that D of pB is smaller than that of pG, we measured D of various unfolded conformations of PYP using a denaturant. D of PYP decreased sharply at the denaturation transition of PYP. Furthermore, the population grating signal under the fully denatured PYP condition can be fitted well by a single exponential function. This fact indicates that D of PYP with the trans form of the chromophore is the same as that with the cis form. This is sharply in contrast to the native PYP, in which D of pG is different from that of pB. The difference in D between pG and pB comes from the different protein structure. These facts clearly indicate that D is determined by the protein conformation in that solution.

In the characterization of native and non-native states of proteins in solution, a measurement of the molecular dimensions of the system is valuable. A measure of the average dimensions of the conformational ensemble can give information about the nature of the structures adopted by the polypeptide chain. D can probe the average dimension and the coupling of the local and global conformational properties of these unfolded and partly folded species. According to the time-resolved crystallography, the guanidinium group of Arg52 moves toward solvent in the pB state and phenolic oxygen of the head part of the chromophore moves largely from the protein core; as a result, it is solvent-exposed and protonated. This change will increase the protein–water interaction, which could be a cause of the slower diffusion constant of the pB species. However, as long as the change is localized around the chromophore, D may not be changed so much. We suppose that the surface of the whole protein dramatically changes to hydrophilic character by the transformation from pG to pB.

D cannot represent the real radius of the diffusing species but this 'hydrodynamic radius' gives us an intuitive sense of the radius and the interaction. One of methods to connect the intermediate species and the unfolded structure is to use the compact factor C introduced by Wilkins et al.,[61] which is

$$C = (r_h{}^D - r_h)/(r_h{}^D - r_h{}^N) \quad (17)$$

where $r_h{}^D$ and $r_h{}^N$ are the hydrodynamic radii for the native and fully denatured states, respectively, and r_h is the experimentally determined hydrodynamic radius. According to this definition, the protein with the same molecular radius as a native state will have $C = 1.0$ and those with a radius the same as a fully denatured state will have $C = 0$. With a slight modification based on the Stoke–Einstein relationship, C can be equivalently defined as

$$C = (1/D^D - 1/D)/(1/D^D - 1/D^N) \quad (18)$$

where the superscripts of D have the same meaning as above. From this equation, we can say that pB state possesses about 14% unfolded structure compared with pG.

The other argument is related with the surface corrugation and roughness of globular proteins. Choi et al. showed that the magnitude of structural fluctuation and the coefficient of self-diffusion vary with the size of solvent molecules and correlate nicely with the correlation dimensions of the protein by using molecular dynamics simulations.[62] Correlation dimension D_2 is a parameter describing the surface roughness of globular protein molecules, which depends on the size of a guest molecule approaching them. The larger D_2 is, the smaller the diffusion coefficient is. Based on this consideration, the smaller D of pB means that the surface becomes more rough in pB than in pG. This surface roughness should be related with the loosened structure of the pB states as suggested in the above sections.

2-3. Carboxymyoglobin. The relationship between the structural properties of proteins and their reactions is essential for understanding of the protein biological functions. Myoglobin (Mb) has been used as a model system for experimental and theoretical studies of such kinetics–structural relationship. A heme is embedded within the protein and a small ligand (e.g., O_2, CO, NO) is reversibly bound to the sixth coordination site, on the distal side, of the heme. By photoexcitation of the heme, the ligand–metal bond is photodissociated. Since there is no route prepared to pass the ligand through the protein to the outer solvent, the protein structure has to change if the ligand is removed from the protein. This photoreaction can be used, therefore, to trigger a perturbation to the protein by pulsed laser light.

Extensive research has been conducted to understand the dissociation kinetics and subsequent protein deformation.[64–82] Studies of the reaction kinetics at low temperatures showed that there are several intermediates during the course of the overall process from the ligand–metal bond dissociation to the ligand escape from the protein. However, at ambient temperature in water, the kinetics and the features of the multiple intermediate states have not been elucidated well except for a 180 ns geminate recombination kinetics.[67] Furthermore, although the absorption spectroscopic studies revealed structural changes around the heme chromophore, the structural change in the other part, in particular the dynamics of the protein structure has been less clear. Information regarding the energies of the intermediates is very important, but our knowledge is very limited even after the long history of the Mb studies. These difficulties may be solved by using a time-resolved spectroscopy that does

not use the optical transition of the heme. Time-resolved PA method is one of such techniques. Peters and coworkers used this method to study the Mb dynamics.[81,82] From the analysis of the waveforms at various temperatures, the presence of an additional intermediate species was suggested. However, because of inherent limitations of the PA method as described in section 2, the kinetics is not fully resolved. We have applied the time-resolved thermodynamical measurements for this ligand dissociation reaction of carboxymyoglobin (MbCO).

(a) TG Signal of MbCO: The transient absorption signal after the photoexcitation of MbCO rises within our time resolution (10 ns) and shows a weak (ca. 4%) decay component with a lifetime of 180 ns, which represents the geminate recombination kinetics. The signal stays almost constant during microsecond time scale and decay to the baseline with a lifetime of ca. 3 ms by a bimolecular recombination. The time profile of the TG signal shows more complex features.[83–85] Figure 8 depicts the TG signal of sperm whale MbCO in 10 mM Tris buffer at 25 °C.[85] The TG signal rises within the excitation pulse width, followed by a decay component. The signal then shows a growth–decay–growth curve within a few ten μs. On a longer time scale, the signal again rises during several hundred microseconds and finally decays to the baseline with a lifetime of several milliseconds. For comparison, we used malachite green (MG) as a calorimetric reference sample. The photophysical process of MG has been completely investigated and it is well known that all of the photon energy is released to solution much faster than our pulse width. The decay of the TG signal from MG is due to the thermal diffusion and the rate is given by $2D_{th}q^2$ [Eq. 7]. The TG signal of MbCO which decays with a similar rate to that from the reference sample (Fig. 8) should be attributed to the thermal grating component.

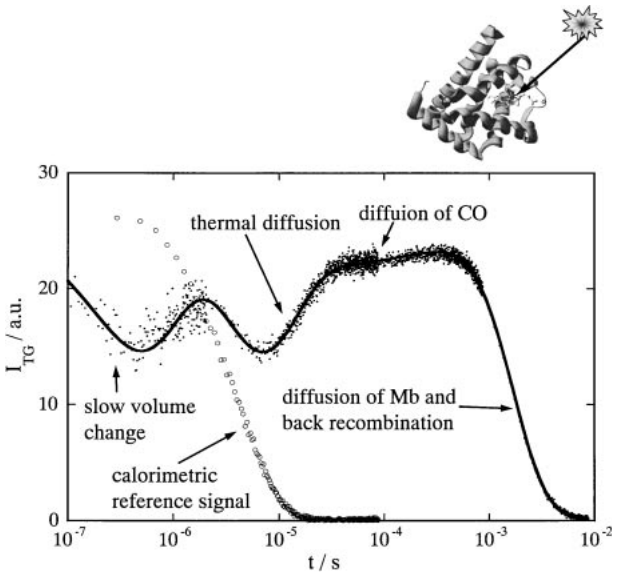

Fig. 8. The observed TG signal (dotted line) after the photodissociation of SW MbCO in 10 mM Tris buffer at 25 °C, and the fitted line (solid line). The decaying signal (open circles) represents the TG signal of Malachite green (MG) in aqueous solution measured under the same condition. The assignments of the kinetic components are labeled in the figure.

In this photodissociation reaction, three species: MbCO, Mb, and CO can contribute to the species grating signal. MbCO and Mb produce both the phase and amplitude gratings at the probe wavelength of 840 nm. On the other hand, CO only contributes to the phase grating, because there is no absorption band at this probe wavelength. We found that the time profile during 10^{-7}–10^{-4} s range can be reproduced very well with Eq. 19:[83,85]

$$\begin{aligned} I_{TG}(t) = \alpha[&\delta n_s \exp(-k_s t) + \delta n_{th} \exp(-D_{th}q^2 t) \\ &+ \delta n_{CO} \exp(-k_{CO} t) + \delta n_{Mb} \exp(-k_{Mb} t)]^2 \\ &+ \beta(\delta k_g \exp(-k_g t) + \delta k_{Mb} \exp(-k_{Mb} t))^2 \end{aligned} \quad (19)$$

where k_s denotes a rate constant of the first decaying component. These δn_{spe} and δk_{spe} are the origin of the time development on the longer time scale ($t > 10^{-4}$ s). The second term (δn_{th}) of the right hand side of Eq. 19 represents the thermal grating component. The first decay-rise curve originates from the interference between δn_s and δn_{th}. The background intensity at the bottoms of these interference dips reflects the δk_{spe} component, which can be attributed to the absorption change of the band III due to deoxyMb at this wavelength. The first term in the amplitude grating term represent the geminate recombination process with the rate constant of k_g. Using a least squares fitting, the signal can be separated into δn and δk contributions and the decay rate constants k_{CO} and k_{Mb} are thus determined. The rate constant of k_{Mb} and k_{CO} should be given by $D_{Mb} + k_{back}$ and $D_{CO} + k_{back}$, respectively, where k_{back} is the ligand recombination rate (Mb + CO → MbCO). Because the diffusion constant of CO should be much larger than those of Mb or MbCO ($D_{CO} \gg D_{Mb}$), the fast decaying component ($\sim$ ms) is attributed to the species grating due to CO ($k_{CO} = D_{CO} + k_{back}$) and the slower one ($\sim$ ms) to Mb and MbCO ($D_{MbCO} \sim D_{Mb}$). The plot of the decay rate constants, k_{CO} and k_{Mb} as a function of q^2 was linear as expected. The intercept of the plot at ${k_{back}}^{-1} = 3$ ms is reasonably close to that measured by the laser flash photolysis experiment probed at 633 nm under the same condition (2.8 ms). The diffusion constants of Mb and CO are determined to be $D_{CO} = (2.6 \pm 0.3) \times 10^{-9}$ m^2 s^{-1} and $D_{Mb} = (1.2 \pm 0.1) \times 10^{-10}$ m^2 s^{-1} from the slope of the plots.

The kinetics with the lifetime of k_s observed in the TG signal certainly indicates the presence of dynamics of MbCO with this rate. However, studies using the transient absorption technique reported so far indicate that the geminate recombination of the CO with a lifetime of 180 ns and a quantum yield of 4% occurs[67] and there is only a minor change (<5%) in visible absorption around 700 ns at 20 °C.[77] Hence we conclude that the observed 700 ns-kinetics in the TG signal is not associated with the absorption change; that is, the population phase grating component (δn_{pop}) and also the amplitude grating signal (δk_{pop}) should be almost constant during this time range. The 700 ns-component should be attributed to the kinetics of the molecular volume change and/or the thermal grating component.

(b) Assignment of the Spectrally Silent Dynamics: This spectrally silent dynamics in the TG signal may be explained by the following two models.[85] First, after the breaking of the Fe–CO bond, the CO is trapped in the heme pocket (Mb:CO). While the 180 ns-kinetics reflects the transfer time of the CO from one heme pocket to another heme pocket (Mb(CO)), the

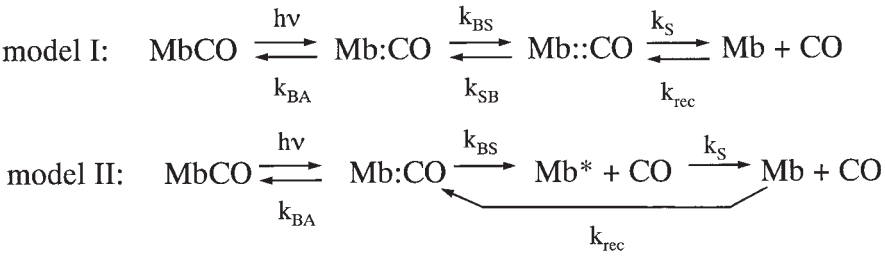

Scheme 1.

700 ns-kinetics observed in the TG signal could be the escaping process of the CO from the second heme pocket to the solvent (Scheme 1, model I). Second, it is possible that there is only one heme pocket inside the protein interior and that the CO diffuses out from the protein with the lifetime of 180 ns. After the escaping process of the CO, the protein structure of Mb* should be changed to the structure of equilibrium deoxyMb. The 700 ns-dynamics may represent the structural relaxation of the protein during this process (Scheme 1, model II).

We examined the dynamics more clearly from the time profiles of the TG signal based on the two models described above. The main difference between these two models is the location of the CO before the 700 ns-dynamics. In model I, the CO is present inside the protein, whereas it exists in the solution phase in model II. Therefore, by examining the species grating signal of CO, we could distinguish these models. For that purpose, we measured the TG signal at a rather low grating wavenumber ($q = 5.4 \times 10^5$ m^{-1}) and a high grating wavenumber ($q = 8.2 \times 10^6$ m^{-1}).

Solving diffusion-rate equations based on the above models, we found that the pre-exponential factor (δn_{CO}) of the $\exp(-D_{CO}q^2t)$ term in a low q region ($k_s \gg D_{CO}q^2$) is given by

$$\delta n_{CO}(low - q) = (1 - \phi_g)\delta n^0_{CO} \quad (20)$$

for models I and II. Here ϕ_g is the quantum yield of the geminate recombination. On the other hand, under the high q condition ($k_s \sim D_{CO}q^2$), δn_{CO} is given by

$$\delta n_{CO}(high - q) = \frac{k_{BS}k_S}{(k_g - D_{CO}q^2)(k_S - D_{CO}q^2)}\delta n^0_{CO} \quad (21)$$

for Model I, and

$$\delta n_{CO}(high - q) = \frac{k_{BS}}{k_g - D_{CO}q^2}\delta n^0_{CO} \quad (22)$$

for Model II. Here, k_g is the rate constant of the geminate recombination. In order to eliminate the unknown quantity δn^0_{CO}, we take a ratio of to $\delta n_{CO}(high - q)$ to $\delta n_{CO}(low - q)$. Using the experimental data $k_{BS} = 5.3 \times 10^6$ s^{-1}, $k_{BA} = 0.24 \times 10^6$ s^{-1}, $k_g = 5.5 \times 10^6$ s^{-1}, $\phi_g = 0.043$,[74] $k_S = 1.4 \times 10^6$ s^{-1} ($= 1/\tau_s$), and $D_{CO}q^2 = 0.19 \times 10^6$ s^{-1} at 20 °C under the condition of $q = 8.2 \times 10^6$ m^{-1}, δn_{CO} is calculated as

$$\frac{\delta n_{CO}(high - q)}{\delta n_{CO}(low - q)} = 1.21$$

for Model I, and

$$\frac{\delta n_{CO}(high - q)}{\delta n_{CO}(low - q)} = 1.04$$

for Model II. The observed TG signal was fitted using the least square method, and the amplitudes of δn_{CO} under the high q conditions are compared. The experimental ratio of $\delta n_{CO}(high - q)$ to $\delta n_{CO}(low - q)$ was

$$\frac{\delta n_{CO}(high - q)}{\delta n_{CO}(low - q)} = 1.2\ (\pm\ 0.01)$$

This ratio is close to what we expect from the calculation based on Model I. Therefore, we clearly conclude that the photodissociated CO escapes from the protein to solvent with the lifetime of 700 ns.

Esquerra et al. also observed a weak component of dynamics with a lifetime of about 500 ns at 26 °C by using transient absorption in the Q-band region (500–650 nm) and magnetic optical ratatory dispersion spectra with a SVD analysis.[77] They discussed several possible origins of the dynamics and concluded that the dynamics may be attributed to the protein relaxation on the distal side of the heme pocket. However, these observations cannot elucidate whether the dynamics with a time constant of about 700 ns is due to the CO escaping from the protein or is due to the protein conformational relaxation after CO escapes to the solvent. Moreover, since the absorption change in Soret band comes from the difference in absorbance between bound state and two non-bound states with different deoxyheme conformations, it can not distinguish the conformational difference in different CO position states. On the other hand, our study clearly assigned the 700 ns-dynamics in the TG signal to the CO releasing. If the weak 500 ns-component in the absorption spectra change at 26 °C is the same process as the 700 ns-dynamics at 20 °C in the TG signal, we can conclude that the CO escaping process from the protein to the solvent weakly change the heme absorption spectrum.

(c) Energies, Volume Changes, and the Kinetics: From the magnitude of the absolute thermal grating signal intensity, we determined the enthalpy change of the reaction for MbCO → Mb + CO. The absolute magnitude of the signal intensity was calibrated by the thermal grating signal intensity of MG under the same conditions. Using a photon energy of $h\nu =$ 227 kJ/mol, we found that the thermal energy released after the 700 ns-kinetics is $Q = 0.70\ (\pm 0.09)h\nu = 159\ (\pm 20)$ kJ/mol. Since the quantum yield of the photodissociation reaction of MbCO is $\phi = 0.96$,[74] the enthalpies difference between the initial MbCO and the photodissociated species (Mb + CO) is $\Delta H_s = (h\nu - Q)/\phi = 70\ (\pm 20)$ kJ/mol.

The TG signal of MbCO was measured as a function of temperature in the range of 20 °C to −2 °C. Some of the signals are depicted in Fig. 9. Since $|dn/dT|$ of water decreases with decreasing the temperature until $T = 0$ °C, the thermal contribution is expected to become minor at lower temperatures. The

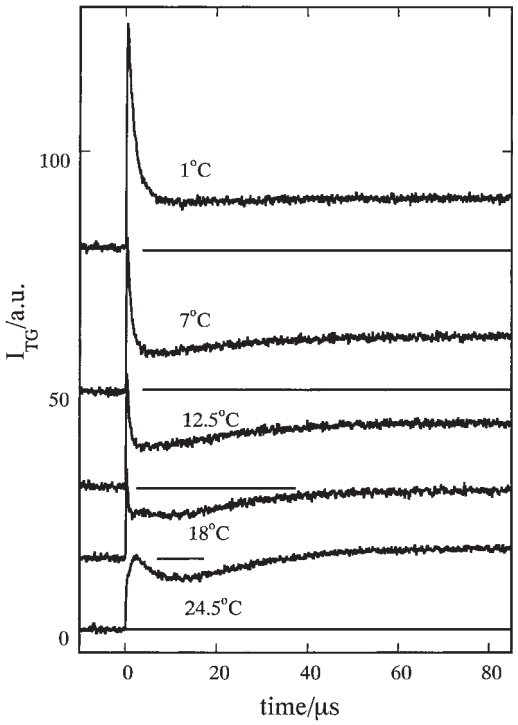

Fig. 9. Temperature dependence of the TG signal after the photoexcitation of MbCO. With deceasing the temperature, the thermal grating signal becomes weak and the volume grating component becomes apparent.

species grating signal intensity (background signal in this time scale) remains almost constant with decreasing temperature. This indicates that the quantum yield of the photodissociation of CO is almost temperature independent in this range. On the other hand, the thermal grating signal intensity diminishes at lower temperatures. The decrease is due to the temperature dependence of dn/dT.

In order to determine the volume change of this reaction, we analyze the TG signal at various temperatures by using the TG setup with the high wavenumber. At $q = 8.4 \times 10^6$ m^{-1}, the thermal grating signal decays with a 70 ns lifetime, which is much faster than the volume change (700 ns at 20 °C). Hence the volume change $\delta n_{\Delta V_s}$ can be directly observed at this high wavenumber experiment without disturbance from the thermal component. The observed temperature dependence of $\delta n_{\Delta V_s}$ indicates that the volume change should depend on the temperature. We found that the volume change with the rate constant of k_s (ΔV_s) is 14.7 cm^3/mol at room temperature and, using this value as a standard, it increases to 16.8 ± 0.3 cm^3/mol at 0 °C.

We used the PA method for the volume change just after the excitation (ΔV_f). To be more accurate than the commonly used approach for the fitting of the PA signal, we fixed most of the parameters and the adjustable parameter was only ΔV_f in this case (Fig. 10). Consequently, we obtained the initial volume change to be $\Delta V_f = -5.2 \pm 3$ cm^3/mol.

We found that ΔV_s at 20 °C is 83% of that at 0 °C, and calculated ΔV_s at 20 °C to be 12 ($\pm$1) cm^3/mol using $\Delta V_s = 14.5$ ($\pm$1.0) cm^3/mol at 0 °C. We calculate thermal energy for slow process (Q_s) by taking into account the temperature-dependent ΔV_s and found that Q_s is 8 ($\pm$5) kJ/mol (exothermic process).

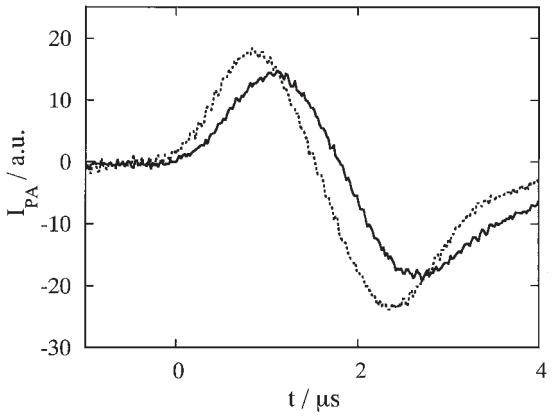

Fig. 10. PA signal of SW MbCO (solid line) in buffer and MG (dotted line) in aqueous solution at 22 °C.

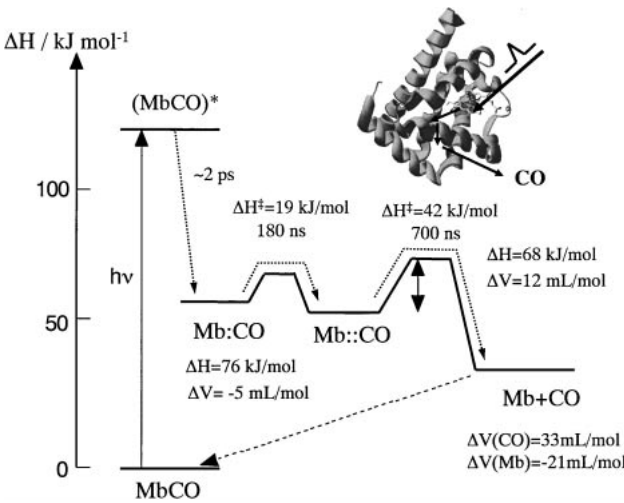

Fig. 11. Energy diagram of photosissociation reaction of MbCO.

With a photon energy of $h\nu = 227$ kJ/mol, the enthalpy of the first intermediate (ΔH_f) and of the slow process (ΔH_s) were determined to be 78 kJ/mol and 70 kJ/mol.

From the temperature dependence of the lifetime τ_s, the enthalpy ($\Delta H^\ddagger$) and entropy ($\Delta S^\ddagger$) of activation can be obtained. The time constant of τ_s is related to $\Delta H^\ddagger$ and $\Delta S^\ddagger$ by the activated complex theory as follows:

$$\ln(k_s h/k_B T) = \frac{\Delta S^\ddagger}{R} - \frac{\Delta H^\ddagger}{RT} \tag{23}$$

where h is the Plank constant and R is the gas constant. From the slope and the intercept of the plot of $\ln(k_s h/k_B T)$ against $1/T$, $\Delta H^\ddagger = 41.9$ ($\pm$1.4) kJ/mol and $\Delta S^\ddagger = 15.4$ ($\pm$4.7) JK/mol were obtained. The energetics and structural dynamics determined in this study are summarized in Fig. 11.

One of interesting observations here is the temperature dependence of ΔV. The difference in α_{th} between the folded and unfolded metmyoglobin was reported to be $\Delta\alpha_{th} = +2.4$ cm^3/mol K.[60] Since the observed temperature dependence of ΔV of this MbCO photodissociation reaction is not so large (0.1 cm^3/mol K) compared with this value, loosening of the protein part should not be so significant after the ligand escape.

However, the temperature dependence is not negligible for the measurement of ΔH and ΔV.

After the photodissociation of CO from the iron, the iron atom moves out of the plane of the pyrrole nitrogen atoms very quickly (~2 ps). The initial structural and enthalpy changes ($t < 10$ ns) are considered to represent the initial movement of the proximal His and the doming process of the heme plane. The 700 ns lifetime at 20 °C observed in the species grating signal is different from the 180 ns kinetics of the geminate pair observed in flash photolysis, suggesting that the intermediate is a species different from the geminate pair.

Peters and co-workers first applied the PA technique to the photodissociation reaction of MbCO.[81,82] Analyzing the PA wave form at various temperatures and assuming that the volume change and the enthalpy change do not depend on temperature, they found that the intermediate species decays with a lifetime of 850 ns for the sperm whale MbCO and 900 ns for the horse MbCO at 20 °C. We believe that the kinetics from the PA and from the TG signals represent the same kinetics, because both techniques detect the structural and energy dynamics in common. The slightly different lifetimes may be caused by the fitting uncertainty of the PA analysis, which involves too many parameters.

Besides the slightly different rates between the PA and our TG study, there is a large difference in ΔH_f. $\Delta H_f = 26$ kJ/mol was obtained for the horse MbCO and $\Delta H_f = 2.5$ kJ/mol for the sperm whale MbCO from the PA analysis. These values are surprisingly smaller than our determined ΔH_f. Westrick et al. postulated the breaking of a Arg45 salt bridge to account for the small ΔH from the PA measurement.[81,82] However, from our results, we definitively showed that this dynamics should be attributed to the ligand escape process. We do not need to consider the salt bridge breaking to account for ΔH. Furthermore, this interpretation was reinvestigated by TG experiments of sperm whale (SW) Mb and horse heart (HH) Mb. There are 21 different amino acids between SW and HH Mb. The most important amino acid of them is Arg45, which is replaced by Lys in HH Mb. Residue 45 forms the salt bridge with the heme 6-propionate side chain in equilibrium deoxyMb and MbCO under the neutral condition.[82,86,87] In spite of these differences, ΔH_f, ΔH_s, and ΔV_s of SW-MbCO are very similar to those of HH-MbCO. It indicates that the salt bridge disruption and other different residues do not contribute so much to these energies and structural changes of this photodissociation reaction. From the observation, the dynamics of the domain that consists of the functionally less important residues can be regarded as rigid body movement.

It is interesting to note that the energy of the first intermediate species determined here (60 kJ/mol) is smaller than the Fe–CO bond enthalpy (105 kJ/mol). This fact indicates that the protein structure is relaxed and stabilized after the CO dissociation within 10 ns. This fast structural relaxation is consistent with the observed volume change in the initial step (-5 cm^3/mol) and also with the observations by Miller and co-workers.[80]

The photodissociation scheme should be described in terms of model I (Scheme 1). The photodissociated CO from the heme is first trapped in a heme pocket, from which the CO can recombine to the heme geminately, and is moved to another pocket with the lifetime of about 180 ns. From the second pocket, the CO is escaped to the solvent phase with the lifetime of 700 ns. The intermediate species of CO in the second pocket is far from the heme and cannot be observed strongly in the absorption change of Soret band. It is because the CO in the second pocket cannot rebind to the heme or the geminate recombination rate from the second pocket is too slow compared with the escape rate to be detected.

Where are these pockets located? The X-ray crystallographic study by Tilton et al. showed that there are four cavities in which Xe binds with high affinity in the protein.[68] One of them near the ligand binding site, which is called Xe$^{(4)}$, is known as the CO docking site.[71,89,90] The IR study by Lim et al.,[89] the MD simulation by Sassaroli and Rousseau[90] and the time-resolved X-ray study[71] showed that CO is trapped in the Xe$^{(4)}$ site as soon as it photodissociated. Considering these studies, we may attribute the location of the first CO trapped site to Xe$^{(4)}$ site. Although the rate with which CO migrates from the first trap site to the second one has not been known, the intermediate with the lifetime of 700 ns could be Mb with CO in the Xe$^{(1)}$ site. We are recently investigating the role of the Xe$^{(1)}$ site by using the Xe pressure dependence of the thermodynamical properties as well as the ligand escape rate and the results will be published soon.

2-4. Octopus Rhodopsin. Visual pigments called rhodopsins are membrane proteins that consist of the apoprotein, opsin, and the 11-*cis* retinal chromophore, which is covalently attached to the opsins via a protonated Schiff base linkage. Identifying and revealing every intermediate during the photoreaction is one of the most fundamental and important steps. Hence extensive researches have been conducted to study the kinetics by mostly transient absorption spectroscopy of the chromophore. After a rhodopsin is photoexcited, photo-isomerization of 11-*cis* retinal to the all-*trans* form takes place, followed by a series of thermal reactions: Batho → Lumi → Meso → Acid Meta. One of the intermediates interacts with the G protein, resulting in the electrical excitation of a photoreceptor cell.[91,92] After photoexcitation of invertebrate rhodoposin, the final product is a stable pigment with all-*trans* retinal. In octopus rhodopsin, the stable acid metarhodopsin (Acid Meta form) can be converted to the original rhodopsin upon orange light illumination.[92] Spectroscopic methods have been extensively applied to the studies of the photocyclic reaction[93–97] and the intermediates of the reaction seem to be established now. From transient absorptional change, the Acid Meta form, which is produced with the rate of 0.07 μs^{-1}, has been believed to be the final species. However, it is not obvious if the optically detected intermediates are all of the intermediates involved in the reaction, because the absorption detection of the chromophore (retinal) can differentiate only the species that has a different conformation close to the chromophore. It could be possible that another species that cannot be detected by an optical absorption technique exists. We have investigated the dynamics of rhodopsin from a view point of the enthalpy and the volume changes.

(a) Spectral Silent Intermediate: Figures 12(A)–(C) show the time profiles of the TG signals of the octopus rhodopsin (about 80 μM) upon photoexcitation (465 nm) probed at 840 nm at 20 °C with $q^2 = 2.0 \times 10^{12}$ m^{-2}.[98,99] The signal rises within 10 ns after the photoexcitation, followed by a decay with

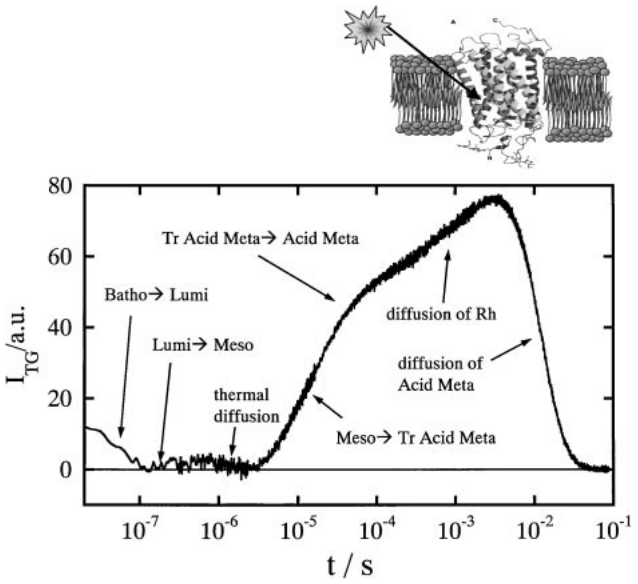

Fig. 12. The kinetics of the TG signal of octopus rhodopsin after 465 nm pulse probed at 840 nm at 20 °C. The assignments of the kinetic components are labeled in the figure.

a tri-exponential function and a single exponential rise within a time window of 10 ns-around 20 μs (Fig. 12(A)). One of the rate constants depends on q^2 but the other does not. The q^2-dependent kinetics are attributed to the thermal grating signal and the q^2-independent kinetics represents the transformation of the Batho to Meso form. The main part of this q^2-independent signal originates from the change of the absorption spectra of Rh (the population grating component). Considering previous studies on the photoreactions of Rh using the transient absorption method, we attributed these dynamics to the reactions of Batho → Lumi → Meso → Acid Meta. The rate constants of the TG signal agree quite well with those determined by the transient absorption method.

After the transformation of Meso to Acid Meta with a lifetime of 23 μs at 20 °C, the TG signal rises with a bi-exponential function on a much longer time scale (Fig. 12(B)) and finally decays to the baseline as a single exponential (Fig. 12(C)). The first rise rate does not depend on q^2 (180 μs at 15 °C and 150 μs at 20 °C); hence it represents the intrinsic kinetics of the protein conformational changes. However, there are no kinetics observed by transient absorption measurements corresponding to this rate. Hence this TG-observed signal is an optically silent transition and the origin of this signal has been attributed to the volume grating component, which comes from the protein structural changes that do not affect the chromophore. This indicates that the parts of the protein distant from the chromophore are still changing even after the changes in the microenvironment around the chromophore are over. Therefore the 'Acid Meta' intermediate should be separated into two, and this new intermediate species was called the transient acid metarhodopsin. Since stable acid metarhodopsin has not been shown to activate G protein, this transient acid metarhodopsin may be responsible for G protein activation.

At the grating wavenumber we usually used ($q^2 = 0.9$–4.0×10^{12} m^{-2}), we observed rise-decay dynamics after this signal, and found that this rate constant depends on q^2. Therefore, these decay rates should represent molecular diffusion processes of the species which exist at this time.

The time-profile of the TG signal over this wide time range (10 ns–100 ms) can be expressed by

$$\begin{aligned} I_{TG}(t) = [&A\exp(-k_1 t) + B\exp(-k_2 t) \\ &+ C\exp(-D_{th}q^2 t) + D\exp(-k_3 t) \\ &+ E\exp(-k_4 t) + F\exp(-D_5 q^2 t) \\ &+ G\exp(-D_6 q^2 t)]^2 \end{aligned} \quad (24)$$

where A–G are pre-exponential factors of these exponential terms: $k_1 > k_2 > k_3 > k_4$ and $D_5 > D_6$. As described above, k_1–k_4 correspond to the rate constants of the Batho → Lumi → Meso → Transient Acid Meta → Acid Meta processes, respectively. From the measurements at various q^2, D_5 and D_6 are determined to be 0.93×10^{-10} m^2/s and 0.27×10^{-10} m^2/s.

(b) Enthalpy Changes: The enthalpies of unstable intermediates have been measured by the cryogenically trapping method. However, as stated in the introduction, the conformation and the energies of the trapped species could be different from those appearing during the biological reaction. We have measured the enthalpy changes of intermediate species at physiological temperatures using the time-resolved technique. The origin of the thermal grating signal is the thermal energy due to the non-radiative transition and the enthalpy changes accompanying the photolysis of octopus rhodopsin. Measuring the time profile of the thermal grating signal of the photochemical sequence of octopus rhodopsin, we determined the enthalpies of these intermediates step by step from the intensities of the signals. From the experimentally determined ratio δn_{th}(Rh*-Batho)/δn_{th}(reference) = 0.72, δn_{th}(Rh*-Lumi)/δn_{th}(reference) = 0.76, δn_{th}(Rh*-Meso)/δn_{th}(reference) = 0.93 and $F = 0.5$,[100] we obtained $\Delta H_{Batho} = 146 \pm 15$ kJ/mol, $\Delta H_{Lumi} = 122 \pm 17$ kJ/mol and $\Delta H_{Meso} = 38 \pm 8$ kJ/mol.

The enthalpy of Transient Acid Meta was determined by using the TrL method. The ratio of the thermal lens signal of the rhodopsin sample and that of the reference was δn_{th}(Rh*-Transient Acid Meta)/δn_{th}(reference) = 0.98. Therefore, the enthalpy of the Transient Acid Meta was determined to be 12 ± 5 kJ/mol. The activation barriers were determined from the temperature dependence of the rate constants. The enthalpies determined for these species are summarized in Fig. 13.

Upon photoexcitation, the initial event in visual pigments is the isomerization of the retinal chromophore from 11-*cis* to all-*trans* form. This isomerization is very fast; it occurs within 400 fs in octopus rhodopsin.[94] The ΔH (ΔH_{Batho}) and ΔV (ΔV_{Batho}) of the Batho determined by TG and PA measurements, are 146 ± 15 kJ/mol and $+32 \pm 3$ cm^3/mol, respectively. Since the energy of the lowest excited state of bovine Rh is 222 kJ/mol (Guzzo and Pool, 1968), only 35% of this energy is released in the formation of Batho. It should be noted that this ΔH_{Batho} value at physiological temperature agrees well with that determined by the cryogenically trapping method ($\Delta H_{Batho} = 130.5$ kJ/mol at −195 °C).[18] This good agreement may indicate that most of the excitation energy is stored by the distorted retinal and its interaction with the surrounding protein at both physiological temperatures and low temperatures. In other words, this correspondence suggests that the structural changes during the step of Rh to Batho are localized around

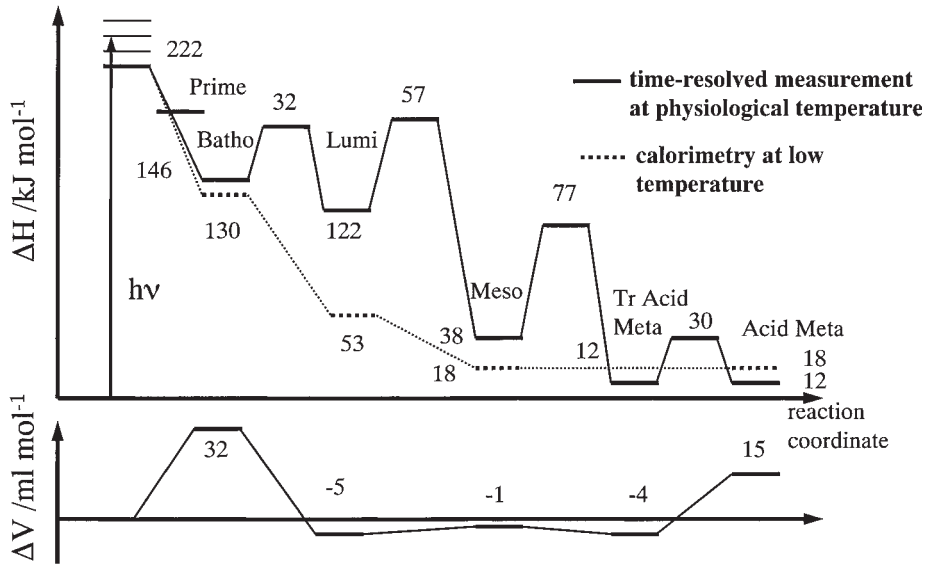

Fig. 13. Upper: Comparison of the relative enthalpies of the various photointermediates of octopus rhodopsin at physiological temperatures (solid horizontal lines) with those measured at low temperature (dotted lines).[18] The activation enthalpies between these steps, measured by the temperature dependence of the reaction rates are also shown in the figure. Lower: Volume changes along this reaction coordinate.

the chromophore. This change was attributed to the change of the electrostatic interaction between the protonated Schiff base and a counter ion. It is very plausible that the isomerization of the retinal results in steric hindrance in the binding pocket. These strains may be the source of the high free energy of this state.

ΔH of Lumi (ΔH_{Lumi}) and Meso (ΔH_{Meso}) at physiological temperatures is dramatically decreased between Lumi and Meso. Comparing these values with those determined by the cryogenic trapping method ($\Delta H_{\text{Lumi}} = 53.3$ kJ/mol at -115 °C and $\Delta H_{\text{Meso}} = 18$ kJ/mol at -65 °C),[18] one should notice that ΔH_{Lumi} is very different from the value detected here. This difference could mean that the conformational change depends on temperature; that is, the structure around the chromophore could be similar for the cryogenic and the physiological temperatures as indicated by the absorption spectrum, but the conformation apart from the chromophore may be different. In other words, the conformational change during the Batho → Lumi process is more or less global. On the other hand, the enthalpy of Meso is similar at both temperatures (20 °C and -65 °C).

(c) Volume Change: The volume change of each photoreaction step was determined by using the PA method. The PA signal intensity represents the thermal expansion and the molecular volume changes. We fitted the PA signal that was measured at very low excitation laser power (about 1 μJ/pulse) the same as for the TG method to avoid the multi-photon excitation. We obtained as $\Delta V_{\text{Rh-Batho}} = +32 \pm 3$ cm^3/mol, $\Delta V_{\text{Batho-Lumi}} = -5 \pm 3$ cm^3/mol, $\Delta V_{\text{Lumi-Meso}} = -1 \pm 1$ cm^3/mol and $\Delta V_{\text{Meso-Transient Acid Meta}} = -4 \pm 3$ cm^3/mol. Finally, the volume change associated with the transformation of Transient Acid Meta → Acid Meta was measured by the TG method as the volume grating component. The volume change was $\Delta V = +13 \pm 3$ cm^3/mol. The relative enthalpies of the octopus rhodopsin photointermediates for the ground state rhodopsin and reaction volume changes for the corresponding transition determined in this study are summarized in Fig. 13.

The observed volume change in the transformation of Rh* to Batho is quite large compared with those of the other subsequent processes (except the last Transient Acid Meta → Acid Meta one). It is interesting to note that the initial steps of two other photoreceptor systems also showed a positive volume change (Rh* → Batho of bovine rhodopsin is 5 cm^3/mol,[101] sensory rhodopsin I is 5.5 cm^3/mol).[102] This change should be related to the isomerization of the retinal because, as discussed above, the structural changes in this step are rather localized around the chromophore. Since the dipole moment of retinal Schiff base does not significantly change upon isomerization,[103] the observed volume change is not due to an electrostriction effect. Losi et al. speculated that the volume expansion reflects the partial disruption of weak interactions (e.g., hydrogen bonding) between the chromophore and the adjacent amino acid residues.[102] Considering the structural information obtained so far, we think that the volume change could be related to the structural changes that induce the energetic stabilization, such as the distortion of the retinal and the Schiff base linkage, alteration of the electrostatic interaction, and change of steric interactions in the binding pocket.

While a small volume change was observed for Meso → Transient Acid Meta (-4 ± 3 cm^3/mol), a relatively large volume change was detected ($+13 \pm 3$ cm^3/mol) for Transient Acid Meta → Acid Meta. This observation supports the idea that the absorption change occurs first by a slight adjustment of the amino acid residues around the chromophore, and subsequently a large scale change takes place far from the chromophore. This large volume change was speculated to be the movement of the helices. It is interesting to be noted that no enthalpy change was detected during this process in spite of the large volume change. Therefore, entropy should drive this process.

3. Conclusion

In this Account, I described some applications of the time-resolved thermodynamical measurements to biological protein reactions: photocycyle of PYP, ligand dissociation reaction of MbCO, and photoreaction of rhodopsin. The volume changes, enthalpy changes, thermal expansion coefficient changes, and the translational diffusion coefficients of transient species have been measured in time-domain without any assumption during these protein reactions. Compared with the traditional techniques, such as the temperature dependence or pressure dependence measurement of the equilibrium constants, this time resolved technique has many unique advantages. One of them is that the thermodynamical changes detected by this method is truly the properties along the reaction coordinate. This advantage may be apparent if one considers that the temperature or pressure affects chemical reactions in many ways. For instance, several solvent parameters affecting the reactions, e.g., the dielectric constant and the viscosity, may be influenced by an increase in pressure or temperature, and it may be difficult by means of high-pressure technique or temperature variation methods to relate the structural or energy change to the actual molecular volume or enthalpy changes. Let us consider a case in which the lifetime of a precursor excited state of a photochemical reaction is pressure-dependent through the variation of the phonon density in the system. The pressure dependence should be analyzed in terms of the phonon density and the mechanism of the nonradiative transition, but not by 'the molecular volume'. In such circumstances, the pressure dependence of the reaction rate cannot be directly related to the volume change of the reaction. Furthermore, one may encounter a similar situation for many protein reactions. Because protein conformation is sensitive to the pressure or temperature, these parameters affect the reaction (such as the equilibrium constant) not only through the reaction itself but also through the change in conformation. One may measure an apparent 'reaction volume' or 'enthalpy change', but, again, these values could not be intrinsic reaction volume or enthalpy change along the reaction coordinate. On the other hand, the properties measured without changing any external properties should reflect the characters of the reaction itself. This technique is also powerful for revealing spectrally silent processes during the reactions, as demonstrated in some reactions in this Account. This merit is particularly useful for protein reactions, because spectrally active change is limited only a small region around the chromophore. Thus the dynamics in the other large conformational area is difficult to detect by the optical transition of the chromophore.

A part of this study was supported by the Grant-in-Aid (No. 13853002) from the Ministry of Education, Culture, Sports, Science and Technology. The author is deeply indebted to co-authors of the papers contained in this Account.

References

1 P. A. Rock, "Chemical Thermodynamics," Mill Valley (1983).

2 K. G. Denbigh, "The Principle of Chemical Equilibrium," Cambridge University Press (1971).

3 T. Asano and W. J. LeNoble, *Chem. Rev.*, **78**, 407 (1978).

4 R. van Eldik, T. Asano, and W. J. LeNoble, *Chem. Rev.*, **89**, 549 (1989).

5 A. Drlijaca, C. D. Hubbard, R. van Eldik, T. Asano, M. V. Basilevsky, and W. J. LeNoble, *Chem. Rev.*, **89**, 549 (1989).

6 E. L. Cussler, "Diffusion," Cambridge University Press (1984).

7 T. J. V. Tyrrell and K. R. Harris, "Diffusion in Liquids," Butterworths, London (1984).

8 M. Terazima, *Chem. Phys.*, **189**, 793 (1994); M. Terazima, *J. Chem. Phys.*, **105**, 6587 (1996); M. Terazima, *J. Chem. Phys.*, **104**, 4988 (1996); T. Okazaki, N. Hirota, and M. Terazima, *J. Phys. Chem. A*, **101**, 650 (1997); M. Terazima, M. Takezaki, S. Yamaguchi, and N. Hirota, *J. Chem. Phys.*, **109**, 603 (1998); M. Terazima, *Chem. Phys. Lett.*, **305**, 189 (1999); T. Okazaki, N. Hirota, and M. Terazima, *J. Chem. Phys.*, **110**, 11399 (1999); T. Okazaki, N. Hirota, T. Nagata, A. Osuka, and M. Terazima, *J. Am. Chem. Soc.*, **121**, 5079 (1999); T. Okazaki, N. Hirota, T. Nagata, A. Osuka, and M. Terazima, *J. Phys. Chem. A*, **103**, 9591 (1999).

9 M. Terazima, T. Hara, and N. Hirota, *Chem. Phys. Lett.*, **246**, 577 (1995).

10 T. Hara, N. Hirota, and M. Terazima, *J. Phys. Chem.*, **100**, 10194 (1996).

11 M. Terazima and N. Hirota, *J. Chem. Phys.*, **98**, 6257 (1993); M. Terazima, K. Okamoto, and N. Hirota, *J. Phys. Chem.*, **97**, 13387 (1993); K. Okamoto, N. Hirota, and M. Terazima, *J. Phys. Chem. A*, **101**, 5380 (1997); M. Terazima, K. Okamoto, and N. Hirota, *J. Chem. Phys.*, **102**, 2506 (1995); K. Okamoto, M. Terazima, and N. Hirota, *J. Chem. Phys.*, **103**, 10445 (1995); K. Okamoto, N. Hirota, and M. Terazima, *J. Phys. Chem. A*, **102**, 3447 (1998); Y. Kimura, D. Kanda, M. Terazima, and N. Hirota, *J. Phys. Chem. B*, **101**, 4442 (1997); K. Okamoto, N. Hirota, and M. Terazima, *J. Chem. Soc., Faraday Trans.*, **94**, 185 (1998); K. Okamoto, N. Hirota, and M. Terazima, *J. Phys. Chem. A*, **101**, 5269 (1997); A. Ukai, N. Hirota, and M. Terazima, *Chem. Phys. Lett.*, **319**, 427 (2000); A. Ukai, N. Hirota, and M. Terazima, *J. Phys. Chem. A*, **104**, 6681 (2000).

12 M. Terazima, *Bull. Chem. Soc. Jpn.*, **74**, 595 (2001).

13 M. Terazima, *Acc. Chem. Res.*, **33**, 687 (2000).

14 P. L. Privalov and N. N. Khechinashvili, *J. Mol. Biol.*, **86**, 665 (1974); *Biophys. Chem.*, **100**, 367 (2003).

15 K. Heremans and L. Smeller, *Biochim. Biophys. Acta*, **1386**, 353 (1998).

16 T. V. Chalikian and K. J. Breslauer, *Biopolymers*, **39**, 619 (1996).

17 A. Cooper, *Nature*, **282**, 531 (1979); A. Cooper, *FEBS Lett.*, **123**, 324 (1981).

18 A. Cooper, S. F. Dixon, and M. Tsuda, *Eur. Biophys. J.*, **13**, 195 (1986).

19 K. A. Bagley, L. Eisenstein, T. G. Ebrey, and M. Tsuda, *Biochemistry*, **28**, 3366 (1989).

20 H. Deng, D. Manor, G. Weng, P. Rath, Y. Koutalos, T. Ebrey, R. Gebhard, J. Lugtenburg, M. Tsuda, and R. H. Callender, *Photochem. Photobiol.*, **54**, 1001 (1991); H. Deng, D. Manor, G. Weng, P. Rath, Y. Koutalos, T. Ebrey, R. Gebhard, J. Lugtenburg, M. Tsuda, and R. H. Callender, *Biochemistry*, **30**, 4495 (1991).

21 C. K. N. Patel and A. C. Tam, *Rev. Mod. Phys.*, **53**, 517 (1981); A. C. Tam, *Rev. Mod. Phys.*, **58**, 381 (1986).

22 "Progress in Photothermal and Photoacoustic Science and Technology," Vol. I (Principles and Perspectives of Photothermal and Photoacoustic Phenomena) and Vol. III (Life and Earth

Science), ed by A. Mandelis, P. Hess, SPIE (1997).
23 S. E. Braslavsky and G. E. Heibel, *Chem. Rev.*, **92**, 1381 (1992).
24 D. P. Almond and P. M. Patel, "Photothermal Sciece and Techniques," Chapman & Hall, London (1996).
25 "Photothermal Investigations of Solids and Fluids," ed by J. A. Sell, Academic, London (1989).
26 J. B. Callis, W. W. Parson, and M. Gouterman, *Biochim. Biophys. Acta*, **267**, 348 (1972).
27 L. Landau and E. Lifsitz, "Statistical Physics, Theoretical Physics," Pergamon Press, Oxford (1969), Vol. 5.
28 K. Heremans and L. Smeller, *Biochim. Biophys. Acta*, **1386**, 353 (1998).
29 H. J. Eichler, P. Gunter, and D. W. Pohl, "Laser Induced Dynamic Gratings," Springer-Verlag, Berlin (1986).
30 M. D. Fayer, *Annu. Rev. Phys. Chem.*, **33**, 63 (1982); R. J. D. Miller, *Ann. Rev. Phys. Chem.*, **42**, 581 (1991).
31 H. Kogelnik, *Bell. System Tech. J.*, **48**, 2909 (1969).
32 M. Terazima, "Advances in Multiphoton Processes and Spectroscopy," ed by S. H. Lin, A. A. Villaeys, and Y. Fujimura, World Scientific, Shigapor (1996).
33 M. Terazima, *Adv. Photochem.*, **24**, 255 (1998).
34 R. S. Lonhurst, "Geometrical and Physical Optics," 2nd ed, Wiley, New York (1967).
35 J. Morais, J. Ma, and M. B. Zimmt, *J. Phys. Chem.*, **95**, 3885 (1991).
36 R. W. Fessenden, P. M. Carton, H. Shimamori, and J. C. Scaiano, *J. Phys. Chem.*, **86**, 3803 (1982).
37 Y. Hirata and N. Mataga, *Chem. Phys. Lett.*, **193**, 287 (1992).
38 J. J. Grabowski, J. D. Simon, and K. S. Peters, *J. Am. Chem. Soc.*, **106**, 4615 (1984).
39 M. S. Herman and J. L. Goodman, *J. Am. Chem. Soc.*, **111**, 1849 (1989).
40 R. R. Hung and J. J. Grabowski, *J. Am. Chem. Soc.*, **114**, 351 (1992).
41 R. Schmidt and M. Schütz, *Chem. Phys. Lett.*, **263**, 795 (1996).
42 T. E. Meyer, *Biochim. Biophys. Acta*, **806**, 175 (1985).
43 W. W. Sprenger, W. D. Hoff, J. P. Armitage, and K. J. Hellingwerf, *J. Bacteriol.*, **175**, 3096 (1993).
44 G. E. O. Borgstohl, D. R. Williams, and E. D. Getzoff, *Biochemistry*, **34**, 6278 (1995).
45 M. Baca, G. E. O. Borgstahl, M. Boissinot, P. M. Burke, D. R. Williams, K. A. Slater, and E. D. Getzoff, *Biochemistry*, **33**, 14369 (1994).
46 W. D. Hoff, P. Düx, K. Hård, B. Devreese, I. M. Nugteren-Roodzant, W. Crielaard, R. Boelens, R. Kaptein, J. Van Beeumen, and K. J. Hellingwerf, *Biochemistry*, **33**, 13959 (1994).
47 T. E. Meyer, G. Tollin, J. H. Hazzard, and M. A. Cusanovich, *Biophys. J.*, **56**, 559 (1989).
48 W. D. Hoff, I. H. M. Van Stokkum, H. J. Van Ramesdonk, M. E. Van Brederode, A. M. Brouwer, J. C. Fitch, T. E. Meyer, R. Van Grondelle, and K. J. Hellingwerf, *Biophys. J.*, **67**, 1691 (1994); S. Devanathan, A. Pacheco, L. Ujj, M. Cusanovich, G. Tollin, S. Lin, and N. Woodbury, *Biophys. J.*, **77**, 1017 (1999); Y. Imamoto, M. Kataoka, and F. Tokunaga, *Biochemistry*, **35**, 14047 (1996).
49 K. J. Hellingwerf, J. Hendriks, and T. Gensch, *J. Phys. Chem. A*, **107**, 1082 (2003).
50 U. K. Genick, G. E. O. Borgstahl, K. Ng, Z. Ren, C. Pradervand, P. M. Burke, V. Šrajer, T. Teng, W. Schildkamp, D. E. McRee, K. Moffat, and E. D. Getzoff, *Science*, **275**, 1471 (1997).
51 B. Perman, V. Šrajer, Z. Ren, T. Teng, C. Pradervand, T. Ursby, D. Bourgeois, F. Schotte, M. Wulff, R. Kort, K. J. Hellingwerf, and K. Moffat, *Science*, **279**, 1946 (1998).
52 a) P. Düx, G. Rubinstenn, G. W. Vuister, R. Boelens, F. A. A. Mulder, K. Hård, W. D. Hoff, A. R. Kroon, W. Crielaard, K. J. Hellingwerf, and R. Kaptein, *Biochemistry*, **37**, 12689 (1998). b) G. Rubinstenn, G. W. Vuister, F. A. A. Mulder, P. Düx, R. Boelens, K. J. Hellingwerf, and R. Kaptein, *Nat. Struct. Biol.*, **5**, 568 (1998). c) C. J. Craven, N. M. Derix, J. Hendriks, R. Boelens, K. J. Hellingwerf, and R. Kaptein, *Biochemistry*, **39**, 14392 (2000).
53 a) H. Kandori, T. Iwata, J. Hendriks, A. Maeda, and K. J. Hellingwerf, *Biochemistry*, **39**, 7902 (2000). b) R. Brudler, R. Rammelsberg, T. T. Woo, E. D. Getzoff, and K. Gerwert, *Nat. Struct. Biol.*, **8**, 265 (2001). c) A. Xie, L. Kelemen, J. Hendriks, B. J. White, K. J. Hellingwerf, and W. D. Hoff, *Biochemistry*, **40**, 1510 (2001).
54 K. Takeshita, N. Hirota, Y. Imamoto, M. Kataoka, F. Tokunaga, and M. Terazima, *J. Am. Chem. Soc.*, **122**, 8524 (2000).
55 K. Takeshita, Y. Imamoto, M. Kataoka, F. Tokunaga, and M. Terazima, *Biochemistry*, **41**, 3037 (2002).
56 K. Takeshita, Y. Imamoto, M. Kataoka, K. Mihara, F. Tokunaga, and M. Terazima, *Biophys. J.*, **83**, 1567 (2002).
57 M. E. Van Brederode, T. Gensch, W. D. Hoff, K. J. Hellingwerf, and S. E. Braslavsky, *Biophys. J.*, **68**, 1101 (1995).
58 T. Gensch, J. M. Strassburger, W. Gärtner, and S. E. Braslavsky, *Isr. J. Chem.*, **38**, 231 (1998).
59 G. Panick, G. J. A. Vidugiris, R. Malessa, G. Rapp, R. Winter, and C. A. Royer, *Biochemistry*, **38**, 4157 (1999).
60 A. Zipp and W. Kauzmann, *Biochemistry*, **12**, 4217 (1973).
61 D. K. Wilkins, S. B. Gimshaw, V. Receveur, C. M. Dobson, J. A. Jones, and L. J. Smith, *Biochemistry*, **38**, 16424 (1999).
62 J. Choi, H. Kim, and S. Lee, *J. Chem. Phys.*, **109**, 7001 (1998).
63 K. Takeshita, N. Hirota, and M. Terazima, *J. Photochem. Photobio. A*, **134**, 103 (2000).
64 R. H. Austin, K. W. Beeson, L. Eisenstein, H. Frauenfelder, and I. C. Gunsalus, *Biochemistry*, **14**, 5355 (1975).
65 D. A. Case and M. Karplus, *J. Mol. Biol.*, **132**, 343 (1979).
66 D. Beece, L. Eisenstein, H. Frauenfelder, D. Good, M. C. Marden, M. L. Reinish, A. H. Reynolds, L. B. Sorensen, and K. T. Yue, *Biochemistry*, **19**, 5147 (1980).
67 E. R. Henry, J. H. Sommer, J. Hofrichter, and W. A. Eaton, *J. Mol. Biol.*, **166**, 443 (1983).
68 R. F. Tilton, Jr., I. D. Kuntz, Jr., and G. A. Petsko, *Biochemistry*, **23**, 2849 (1984).
69 V. Srajer, L. Reinisch, and P. M. Champion, *J. Am. Chem. Soc.*, **110**, 6656 (1988); R. Elber and M. Karplus, *J. Am. Chem. Soc.*, **112**, 9161 (1990); X. Xie and J. D. Simon, *Biochemistry*, **30**, 3682 (1991).
70 V. Srajer and P. M. Champion, *Biochemistry*, **30**, 1390 (1991); P. M. Champion and J. Raman, *Spectroscopy*, **23**, 557 (1992); I. Schlichting, J. Berendzen, G. N. Phillips, Jr., and R. M. Sweet, *Nature*, **317**, 808 (1994); T. E. Carver, R. J. Rohlfs, J. S. Olson, Q. H. Gibson, R. S. Blackmore, B. A. Springer, and S. G. Sligar, *J. Biol. Chem.*, **265**, 20007 (1990).
71 T. Y. Teng, V. Srajer, and K. Moffat, *Nat. Struct. Biol.*, **1**, 701 (1994); V. Srajer, T. Teng, T. Ursby, C. Pradervand, Z. Ren, S. Adachi, W. Schildkamp, D. Bourgeois, M. Wulff, and K. Moffat, *Sceince*, **274**, 1726 (1996).

72 H. Hartmann, S. Zinser, P. Komninos, R. T. Schneider, G. U. Nienhaus, and F. Parak, *Proc. Natl. Acad. Sci.*, **93**, 7013 (1996).

73 J. Vojtchovský, K. Chu, J. Berendzen, R. M. Sweet, and I. Schlichting, *Biophy. J.*, **77**, 2153 (1999); M. Brunori, B. Vallone, F. Cutruzzolá, C. Travaglini-Allocatelli, J. Berendzen, K. Chu, R. M. Sweet, and I. Schlichting, *Proc. Natl. Acad. Sci. U.S.A.*, **97**, 2058 (2000); A. Ostermann, R. Waschipky, F. G. Parak, and G. U. Nienhaus, *Nature*, **404**, 205 (2000); K. Chu, J. Vojtchovský, B. H. Mcmahon, R. M. Sweet, J. Berendzen, and I. Schlichting, *Nature*, **403**, 921 (2000); Y. Sakan, T. Ogura, T. Kitagawa, F. A. Fraunfelter, R. Mattera, and M. Ikeda-Saito, *Biochemistry*, **32**, 5815 (1993); B. A. Springer, S. G. Sriger, J. S. Olson, and G. N. Phillips, Jr, *Chem. Rev.*, **94**, 699 (1994).

74 A. Ansari, C. M. Jones, E. R. Henry, J. Hofrichter, and W. A. Eaton, *Biochemistry*, **33**, 5128 (1994); D. G. Lambright, S. Balasubramanian, S. M. Decatur, and S. G. Boxer, *Biochemistry*, **33**, 5518 (1994).

75 X. Huang and S. G. Boxer, *Nat. Struct. Biol.*, **1**, 226 (1994); J. S. Olson and G. N. Phillips, Jr, *J. Biol. Chem.*, **271**, 17593 (1996); T. P. Cansgrove and R. B. Dyer, *J. Phys. Chem.*, **100**, 3273 (1996).

76 M. Lim, T. A. Jackson, and P. A. Anfinrud, *Nat. Struct. Biol.*, **4**, 209 (1997); E. E. Scott and Q. H. Gibson, *Biochemistry*, **36**, 11909 (1997); M. Brunori, F. Cutruzzolá, C. Savino, C. Travaglini-Allocatelli, B. Vallone, and Q. H. Gibson, *Biophys. J.*, **76**, 1259 (1999); E. E. Scott, Q. H. Gibson, and J. S. Olson, *J. Biol. Chem.*, **276**, 5177 (2001); M. Brunori and Q. H. Gibson, *EMBO Reports*, **2**, 674 (2001); D. C. Lamb, K. Nienhaus, A. Arcovito, F. Draghi, A. E. Miele, M. Brunori, and G. Ulrich Nienhaus, *J. Biol. Chem.*, **277**, 11636 (2002).

77 R. M. Esquerra, R. A. Goldbeck, D. B. Kim-Shapiro, and D. S. Kliger, *Biochemistry*, **37**, 17527 (1998); D. G. Lambright, S. Balasubramanian, and S. G. Boxer, *Biochemistry*, **32**, 10116 (1993); S. Balasubramanian, D. G. Lambright, M. C. Marden, and S. G. Boxer, *Biochemistry*, **32**, 2202 (1993).

78 M. Mukai, S. Nakashima, J. S. Olson, and T. Kitagawa, *J. Phys. Chem. B*, **102**, 3624 (1998); T. Kleinert, W. Doster, H. Leyser, W. Petry, V. Schwarz, and M. Settles, *Biochemistry*, **37**, 717 (1998); S. Nakashima, T. Kitagawa, and J. S. Olson, *Chem. Phys.*, **228**, 323 (1998); H. Ishikawa, T. Uchida, S. Takahashi, K. Ishimori, and I. Morishima, *Biophys. J.*, **80**, 1507 (2001).

79 T. A. Jackson, M. Lim, and P. A. Anfinrud, Seventh International Conference on Time-Resolved Vibrational Spectroscopy, 9-13, Los. Alamos. Natl. Lab., LA (U.S.A.) LA-13290-C (1995).

80 L. Richard, L. Genberg, J. Deak, H. L. Chiu, and R. J. D. Miller, *Biochemistry*, **31**, 10703 (1992); J. Deak, H. L. Chiu, C. M. Lewis, and R. J. D. Miller, *J. Phys. Chem. B*, **102**, 6621 (1998); G. Dadusc, J. Ogilvie, P. Schulenberg, U. Marvet, and R. J. D. Miller, *Proc. Natl. Acad. Sci. U.S.A.*, **98**, 6110 (2001); J. P. Ogilvie, M. Plazanet, G. Dadusc, and R. J. D. Miller, *J. Phys. Chem. B*, **106**, 10460 (2002).

81 J. A. Westrick, J. L. Goodman, and K. S. Peters, *Biochemistry*, **26**, 8313 (1987); W. P. Leung, K. C. Cho, S. K. Vhau, and C. L. Choy, *Chem. Phys. Lett.*, **141**, 220 (1987).

82 J. A. Westrick and K. S. Peters, *Biophys. Chem.*, **37**, 73 (1990); C. L. Norris and K. S. Peters, *Biophys. J.*, **65**, 1660 (1993); J. A. Westrick, K. S. Peters, J. D. Ropp, and S. G. Sligar, *Biochemistry*, **29**, 6741 (1990).

83 M. Sakakura, S. Yamaguchi, N. Hirota, and M. Terazima, *J. Am. Chem. Soc.*, **123**, 4286 (2001).

84 M. Sakakura, I. Morishima, and M. Terazima, *Biochemistry*, **41**, 4837 (2002).

85 M. Sakakura, I. Morishima, and M. Terazima, *J. Phys. Chem. B*, **105**, 10424 (2001).

86 J. Kuriyan, S. Wilz, M. Karplus, and G. A. Petsko, *J. Mol. Biol.*, **192**, 133 (1986).

87 T. E. Carver, J. S. Olson, J. S. Smerdon, S. Krzywda, A. J. Wilkinson, Q. H. Gibson, R. S. Blackmore, J. D. Ropp, and S. G. Sligar, *Biochemistry*, **30**, 4697 (1991).

88 S. V. Evans and G. D. Brayer, *J. Biol. Chem.*, **213**, 885 (1990).

89 M. Lim, T. A. Jackson, and P. A. Anfinrud, *Science*, **269**, 962 (1995).

90 M. Sassaroli and D. L. Rousseau, *J. Biol. Chem.*, **261**, 16292 (1986).

91 L. Stryer, *Annu. Rev. Neurosci.*, **9**, 87 (1986).

92 M. Tsuda, *Photochem. Photobiol.*, **45**, 915 (1987); M. Tsuda, *Biochim. Biophys. Acta.*, **545**, 537 (1979).

93 M. Nakagawa, S. Kikkawa, T. Iwasa, and M. Tsuda, *Biophys. J.*, **72**, 2320 (1997); H. Ohtani, M. Kobayashi, M. Tsuda, and T. G. Ebrey, *Biophys. J.*, **53**, 17 (1988).

94 M. Taiji, K. Bryl, M. Nakagawa, M. Tsuda, and T. Kobayashi, *Photochem. Photobiol.*, **56**, 1003 (1992).

95 C. Pande, A. Pande, K. T. Yue, R. H. Callender, T. G. Ebrey, and M. Tsuda, *Biochemistry*, **26**, 4941 (1987); H. Deng, D. Manor, G. Weng, P. Rathy, Y. Koutalos, T. Ebrey, R. Gebhard, J. Lugtenburg, M. Tsuda, and R. H. Callender, *Photochem. Photobiol.*, **54**, 1001 (1991).

96 K. A. Bagley, L. Eisenstein, and T. G. Ebrey, *Biochemistry*, **28**, 3366 (1989).

97 S. Masuda, E. Morita, M. Tasumi, T. Iwasa, and M. Tsuda, *FEBS Lett.*, **317**, 223 (1993); S. Nishimura, H. Kandori, M. Nakagawa, M. Tsuda, and A. Maeda, *Biochemistry*, **36**, 864 (1997).

98 Y. Nishioku, M. Nakagawa, M. Tsuda, and M. Terazima, *Biophy. J.*, **80**, 2922 (2001).

99 Y. Nishioku, M. Nakagawa, M. Tsuda, and M. Terazima, *Biophy. J.*, **83**, 1136 (2002).

100 H. Ohtani, M. Kobayashi, M. Tsuda, and T. G. Ebrey, *Biophys. J.*, **53**, 17 (1988).

101 T. Gensch, J. M. Strassburger, W. Gärtner, and S. E. Braslavsky, *Isr. J. Chem.*, **38**, 231 (1998).

102 A. Losi, S. E. Braslavsky, W. Gartner, and J. L. S. Spudich, *Biophys. J.*, **76**, 2183 (1999).

103 S. A. Locknar and L. A. Peteanu, *J. Phys. Chem. B*, **102**, 4240 (1998).

Masahide Terazima was born in 1959 in Kagawa, Japan. He obtained his B.Sc. (1982), M.Sc. (1984), and Ph.D (1987) degrees from Kyoto University. In 1986, he became a research associate in Tohoku University. In 1990, he moved to Department of Chemistry of Kyoto University as a lecturer. He was promoted to an associate professor in 1993 and to a full professor in 2001. He is interested in energetics and molecular dynamics after photoexcitation of (relatively small) organic molecules as well as biological proteins in solution phase using several third-order optical nonlinear spectroscopies. He received the Award of Photochemical Association of Japan in 1999, Japanese IBM award of Science in 2002, and The Chemical Society of Japan Award for Creative Work for 2003.